SATREPS Workshop in Kyoto of
“Integrated Study on Mitigation of Multimodal Disasters Caused by Ejection of Volcanic Products”

March 2016 Bromo

Date: 24-25 October 2016

Venue: Disaster Prevention Research Institute
Kyoto University Uji Campus

SATREPS Workshop in Kyoto of “Integrated Study on Mitigation of Multimodal Disasters Caused by Ejection of Volcanic Products”
Date: 24-25 October 2016
Venue: Renkei-Kenkyu-To Large Seminar Room No.301, Disaster Prevention Research Institute, Kyoto University, Gokasho, Uji, 611-0011, Japan

Day 1. Time: 10:00AM-5:10PM

1.Greeting from Project Leader Masato Iguchi
2. An overview of the SATREPS Project implementation in period of 2014-2016 Kasbani
3.A method for providing multi-hazard information related to sediment disasters during heavy rainfalls Masaharu Fujita
4.Seismic and geodetic preliminary analyses during the short 2015 euptive episode of Semeru volcano and the 2015-2016 non eruptive episode of Guntur Volcano Hendra Gunawan
5.Baseline Analysis of GPS Continnes Data in Sinabung, Semeru, Guntur and Galunggung Volcanos Indonesia Yoga Era Pamitro
6.Process of magma intrusion and effusion at Sinabung volcano, Indonesia, during the period from 2013 to 2016, as revealed from continuous GNSS observation data Kohei Hotta
7.Growth process of the lava dome/flow complex during 2013¬ー2016 at Sinabung Volcano, North Sumatra, Indonesia Setsuya Nakada
8.Historical development and recent status of the ground deformation at Merapi volcano Java Indonesia I Gusti Made Agung Nandaka
9.Combination Model of Spherical Source and Block Movement for Asymmetric Ground Deformation Prior to The Eruptions in 2006 and 2010 at Merapi Volcano Nurnaning Aisyah
10.Volume of pyroclastic flow forecasted by precursory seismicity of Merapi volcano Masato Iguchi
11.Seismic velocity variation associated with the large 2010 eruption of Merapi Volcano Agus Budi Santoso
12.Volcanic earthquake activity analysis and eruption imminent evaluation system using seismic data Haruhisa Nakamichi

13.Rainfall characteristics on the southern flank of Mt. Merapi in Indonesia Yutaka Gonda
14.Radar Information at Mt. Merapi Area and Varius Water & Sediment-related Disasters - Case of 18 June 2016 Rachmad Jayadi
15.Temporal change of infiltration characteristics of volcanic ash layer and its effect on rainfall-runoff processes Shusuke Miyata
16.Real-time lahar hazard map generation using X-MP radar forecast products in Merapi volcano Ratih Indri Hapsari
17.A Dynamic Hazard Level Assessment of Lahar In Mount Merapi Magfira Syarifuddin

Day 2. Time: 9:00AM-5:00PM

18.Integration of monitoring data analysis for volcanic hazard assessment Gede Suantika
19.Examination of characteristics of tilt records associated with volcanic eruption at Sakurajima for development of a prediction model for discharge rate of volcanic eruptions Takeshi Nishimura
20.Spectral ratio analyses of explosion earthquakes at Sakurajima Mohammad Hasib
21.Study on behavior of debris flows containing fine sediment from volcanic region
Kana Nakatani
22.Sensitivity Analysis of Lahar Flow Simulation as Affected by DEM Resolutions - Case of Kali Putih, Mt. Merapi Area Adi Putri Anisa Widowati
23.The Mineralogy of Lahars Deposits in Wlingi reservoir and its Role in Controlling Flushing Efficiency Dian Sisinggih
24.An example of pyroclastic flow hazard mapping at Mt. Merapi by using numerical simulation
Kuniaki Miyanomto
25.Cloud Networks - System, Types and their Management Dicky Hadiyuwono
26.Progress of development of simulation and observation Integrated database system
Makoto Shimomura
27.Utilization of X-band radar information for lahar Early Warning System (EWS) at Mount Merapi
Arif R. Mulyana
28.Installation of Volcanic Ash Dispersion PUFF Model to BMKG Indonesia
Kurniaji
29.Determination of the mass eruption rate for the 2014 Mount Kelud eruption using three-dimensional numerical simulations of volcanic plumes Yujiro Suzuki
30.Comparison of Volcanic Ash Dipersion Using PUFF Model with RGB image from Himawari-8 Data Andersen Panjaitan

31.Three-dimensional view of volcanic ash clouds based on weather radar data
Masayuki Maki
32.Development of Estimating Method for Volcanic Tephra Volume by Meteorological Radar
Satoru Oishi
33.Satreps, from Yogyakarta to National: seed for National-wide implementation
Dwi Kristianto

34. Discussion
35. Closing Remark Kasbani

An Overview of the SATREPS project implementation in period of 2014-2016

Kasbani (CVGHM)

Indonesia lies at the junction of 4 major tectonic plates (Eurasian, Pacific, Australian, and Philippine), that constitute one of the most actively deforming tectonic domain on earth. As a consequence of this geologically active region, major geological disasters have occurred. Of course there are deadly eruptions, including those at Merapi, Kelud, Semeru, Guntur, Galunggung and Sinabung volcanoes. The collaboration Japan-Indonesia in geo-hazard domain under SATREPS Project, comprising 5 working group/sub system and signed in December 2013, involves different government institutions and universities in both Indonesia and Japan, has been developing an integrated system to mitigate many kinds of disasters which are generated by volcanic eruptions at Merapi, Kelud, Semeru, Guntur, Galunggung and Sinabung volcanoes which also extended by rain fall and wind. The acquisition of basic data with the observation system (Group 1), the development of technology/methodology (Group 2, 3 and 4) have already been set up while the designing of system interface (Group 5) is ongoing. Now the SATREPS Project is in the half-way phase. Early warning system will be using and developing real-time measurements-based, including the prediction of volcanic behavior, the quantification of eruptive discharge, and the monitoring of rain fall/ash cloud (Fig. 1) and being integrated to the model simulation engine, database, and interface. This integrated system is an important key to mitigate volcanic and sediment disaster and also for counter measures against volcanic ash for airlines. We expect that the integrated system employed in a form of support system of decision making (SSDM) established for responding to volcanic and sediment hazard mitigation and also be able utilized by disaster management authorities and related organizations in accordance with their administrative role and responsibility.

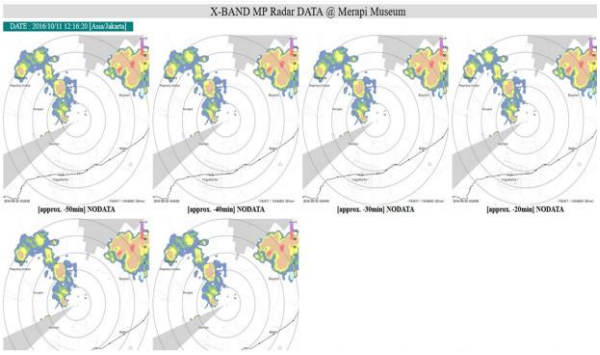

Fig. 1 Rain clouds measurement at Merapi on October 10, 2016 from Group 1.

A method for providing multi-hazard information related to sediment disasters during heavy rainfalls

○Masaharu Fujita, Kazuki Yamanoi (Kyoto U.)

Japanese local governments have a standard warning and evacuation system for sediment disasters based on weather information and sediment disaster warning information. In post-eruption periods, it will be used for debris flows and mudflows. However, it is hard to say that the system is functioning properly. In particular, there is difficulty in the process of issuing evacuation orders after receiving sediment disaster warning information. One of the reasons is that the warning information itself is too vague to imagine the coming disasters.

Sediment disasters due to heavy rainfalls are generally caused by the combination of multi-hazards such as rock falls, flood inundation, shallow landslides, debris flows, deep seated landslides and so on. Various kinds of hazards must happen with different timings and locations in an area where a heavy rainfall continue for a long time. Early evacuation is one of the most effective countermeasures, but multi-hazards always interrupt the evacuation actions. Therefore, it is very important to predict the possible multi-hazards and utilize the multi-hazards information for early evacuation.

The current warning system provides information on the risk of sediment disasters, that the risk is high or low. The similar information is issued for deferent rainfall events. However, the features of multi-hazards in different rainfall events must quite different each other. Therefore, the inhabitants in a high risk area should take an appropriate action considering the feature of multi-hazards in each rainfall event. However, no more information on these things is provided by the current system. This seems to be one of the most important problems in warning and evacuation systems.

We have developed a multi-hazards simulator called 'Storm Induced Multi-Hazards Information Simulator (SiMHiS)'. This simulator can provide real time information on the risk of landslides and overflow from rivers on a basin scale. It consists of a basin model, a slope unit model, a landslide model, a sediment production model, a sediment supply model, a rainfall and sediment runoff model. Rainfall intensity is related to visibility in evacuation actions. Landslides influence evacuation actions by closure of the roads as well as direct damages to residences. Overflow from rivers is related to difficulty in evacuation actions, too. As multi-hazards information, therefore, the risk related to these hazards are predicted.

The simulator was applied to the Hata River Basin. Several rainfall conditions in the simulation and the snake line are shown in Fig. 1. The changes in the risk of landslide and overflow in a unit slope and channel are indicated on the snake lines. Based on these results, the lines of risk level 3 in the residential area are obtained for landslide, overflow and rainfall intensity as shown in Fig. 2. This figure shows that the landslide risk become higher before the snake lines pass the CL. The risk level of overflow increases after the snake lines pass the risk level 3 for landslide, but then decreases and increases again. This feature of overflow risk is related to the process of sediment deposition and erosion in the channels.

The current warning system informs that sediment disasters happen or don't happen in next one or two hours. Nobody knows what kind of risk is coming to them. It leads to more appropriate evacuation if we can realize more detailed information by the presented simulator.

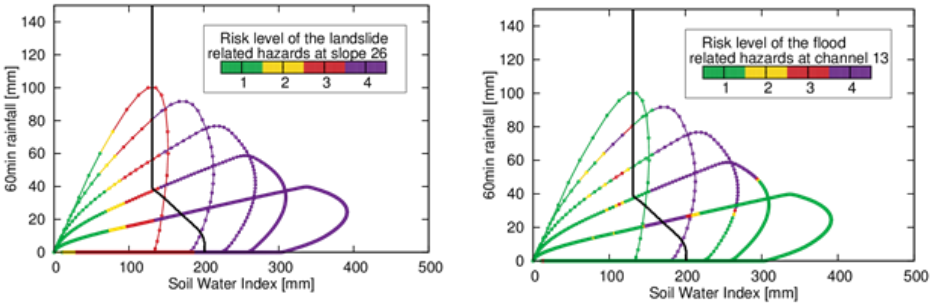

Fig. 1(a) and (b) Process of multi-hazard along snake lines

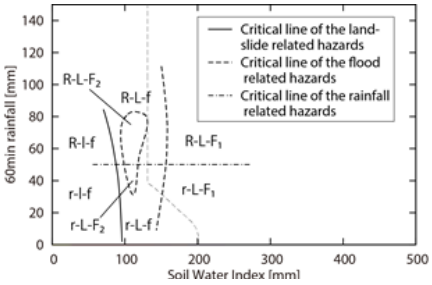

Fig. 2 Multi-hazards information along a snake line by simulation

Seismic and geodetic preliminary analyses during the short 2015 eruptive episode of Semeru volcano and the 2015-2016 non eruptive episode of Guntur volcano

Hendra Gunawan (CVGHM), Ahmad Basuki (CVGHM), Yoga Era Prawiro (CVGHM)

During historical eruption of Semeru volcano at the 2003-2012 period eruption at least there are 8 times eruption which are characterized by lava flow (Fig. 1) and pyroclastic flow (PF) and 3 times short lived explosion. The runout distance of PF varied between 1-4 km descend to Besuk Bang river. There was only one PF which have runout distance 11 km to Besuk Bang river, it occurred in 2003. As long as this eruption period the volcanic tremor showed a good correlation with the ground visual observation at the crater including in the 2015 period. On 8 November 2015, where the crater spewed lava and lava flow, upward gliding harmonic tremor occurred. However the pyroclastic flow occurred only on 13 February 2015 which its runout distance between 4-5 km. The deformation monitoring result using GPS data analysis showed a small variation in the November-December 2015 period.

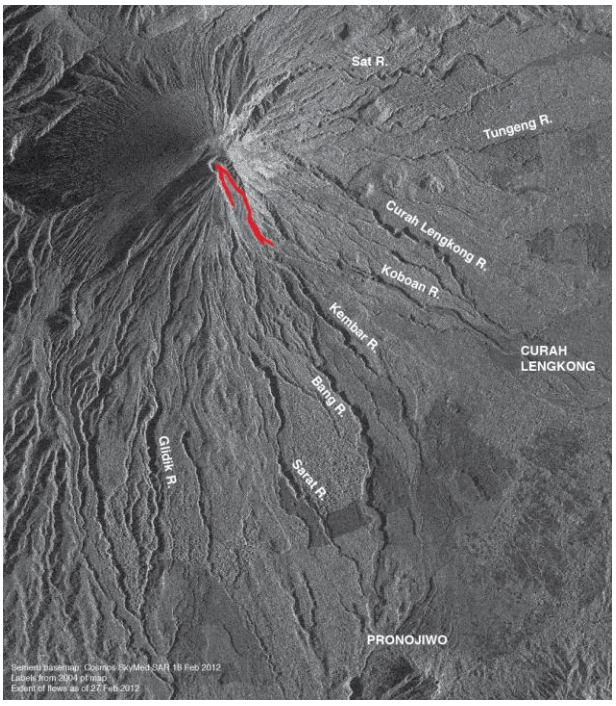

Fig. 1. Lava flow along Besuk Bang river-Semeru volcano. Image from SkyMed SAR taken on 18 February 2012.

Guntur is an active strato volcano which located in West Java Province, Indonesia (60 km to the south of Bandung). Guntur volcano with elevation about 2,249 m above sea level has several cones at summit which form one large group named Guntur volcano. Base on historical records of Guntur volcano, the first eruption was in 1690 and the last was in 1847 which produced lava flow and pyroclastic material. It has been 169 years since the last eruption of Guntur volcano. During this period the volcanic activity data of Guntur volcano show a slow increase in seismic and deformation activity (Fig. 2 and Fig. 3), at least in the period 1990-2016, and .the Guntur's activity level status had been upgraded from Level I into Level II only in 1997 and in 2013.

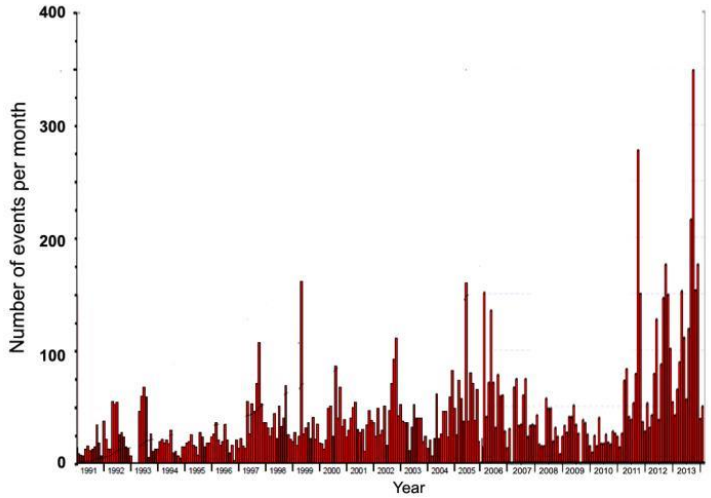

Fig.2 Increasing number of event 1991 - 2013

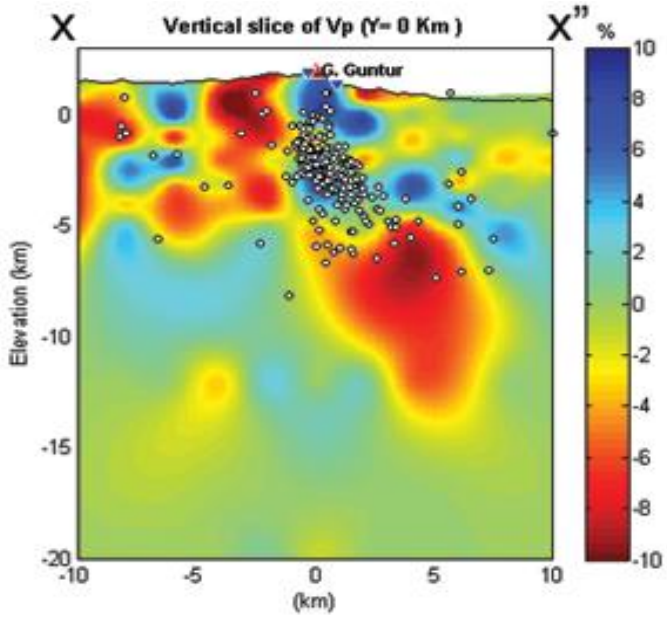

Fig. 3 East-West cross section of Guntur volcano show that high Vp velocity found depth 0 km below Cipanas hotspring, suggesting reservoir area and low Vp velocity found depth of 5 km, suggesting hot materials or fluid (Ahmad Basuki, 2015)

Baselines Analyses of Continues GPS Data in Sinabung, Guntur, Galunggung, Kelud, and Semeru Volcano Indonesia.

Yoga Era Pamitro (CVGHM)

Eruption activity of a volcano is usually preceded by some precursors such as an increase in seismic activity, an increase in the temperature of the hot springs, changes in the composition and strength of gas emissions, as well as deformation of the volcano. To be able to monitor the activity of a volcano, it is important to consider data input from a wide variety of monitoring methods, one of these methods is deformation monitoring using GPS data. This study conducted deformation analysis based on GPS data processed by GAMIT/GLOBK 10.6 software. The data used in this study is including local data from continuous GPS observation stations around Sinabung Volcano, Guntur Volcano, Galunggung Volcano, Kelud Volcano, and Semeru Volcano. While the IGS stations used as a tie point in analyzing the displacement time series are as many as 11 stations. As an illustration Fig. 1a, b, c, d and e shows GPS data analysis at Guntur volcano. Seismic data also used as comparison of the volcanic activity during the period of GPS data processing.

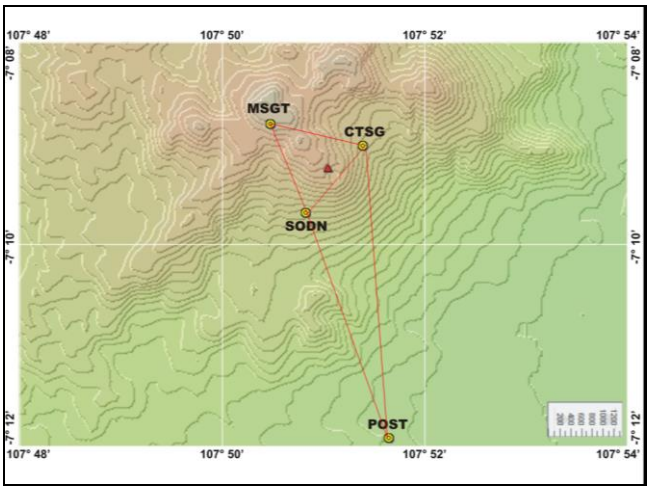

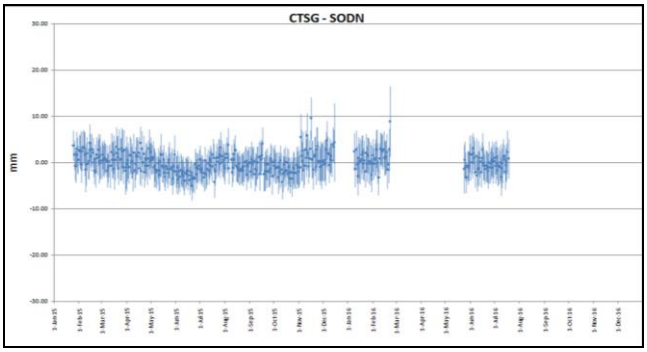

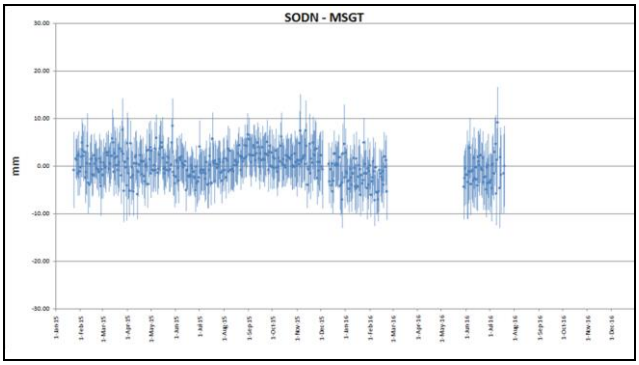

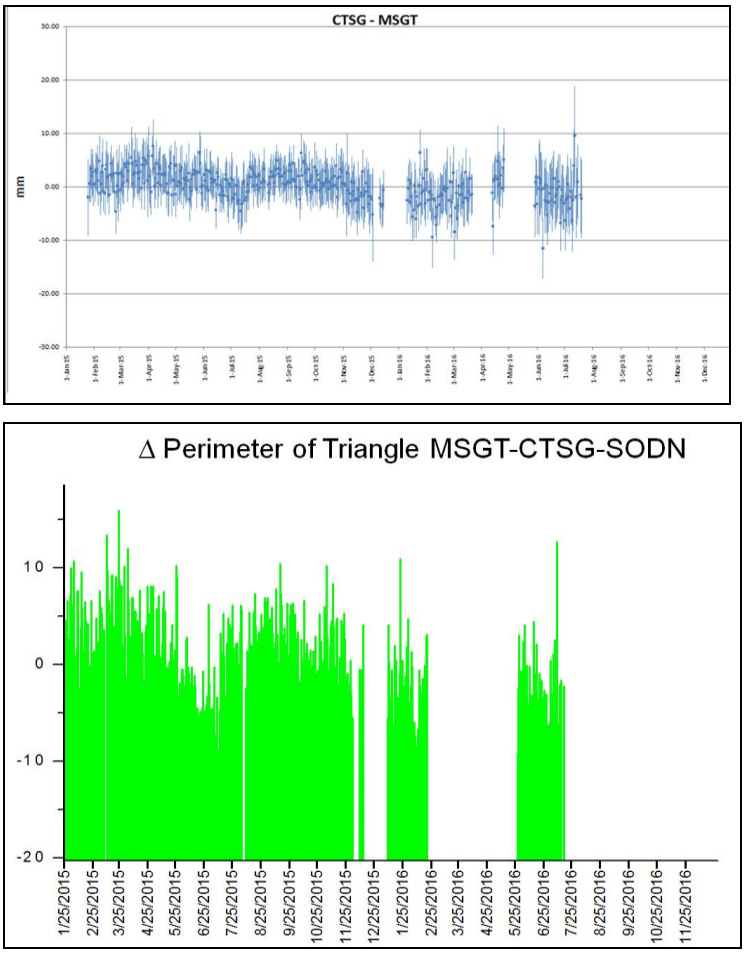

Fig. 1 (a) GPS network at Guntur volcano. (b-d) Baseline of CTSG-SODN station, SODN-MSGT station and CTSG-MSGT station (in mm). (e) Based on the continues GPS data at the station MSGT, CTSG, and SODN of Guntur Volcano, period 1 January 2015 – 19 July 2016, we can notice that the deformation around the summit of Guntur Volcano can be divided into several periods at general. Those periods are 1 Jan 2015 – 25 Mar 2015 (inflation), 25 Mar 2015 – 9 Jul 2015 (deflation), 9 Jul 2015 – 16 Sep 2015 (inflation), and 16 Sep 2015 – 19 Jul 2016 (deflation).

Process of magma intrusion and effusion at Sinabung volcano, Indonesia, during the period from 2013 to 2016, as revealed from continuous GNSS observation data

°K Hotta, M Iguchi, T Ohkura (Kyoto U.), M Hendrasto, H Gunawan, U Rosadi, E Kriswati (CVGHM)

We analyzed continuous data of Global Navigation Satellite System (GNSS) installed at Sinabung to make clear the magma migration process of the activity from 2013. Extension in slope distance before the lava dome appearance in December 2013 and subsequent contraction were detected by GNSS. We divided from June 2013 to January 2016 into Periods 1–4 (Fig. 1). Using a grid search method, we determined location and volume change of a Mogi source for each period.

For the period 1, a deep inflation source was obtained at depth. This indicates deep magma injection started in June 2013 when extension began. For the period 2 when extension rate increased, an inflation source was obtained beneath the summit at a depth of 0.9 km bsl. This indicates magma migration toward shallower accompanied by increase in shallow volcano-tectonic (VT) earthquakes; and finally appeared as the lava dome in December 2013. For the period 3 when extension shifted to contraction, a deflation source was obtained at eastern flank of Sinabung at a depth of 8.4 km bsl. The magma reservoir beneath eastern flank deflated accompanied by frequent magma effusions and pyroclastic flows. For the period 4 when contraction rate decreased, deflation moved away to east-west at a depth of 12.2 km bsl. This indicates deflation reach to the deeper magma reservoir (Fig. 2).

We estimated temporal volume change of the deformation source fixing the location at the position obtained for each period. Volume increase rate increased after vulcanian eruptions in November 2013, which indicates significant magma movement toward the summit. As for the deflation periods, volume change can be approximated as an exponential decay. Deflation from 2014 until middle 2016 is approximately 2/3 of total deflation amount. Current Sinabung deflation is expected to decrease gradually and reach to convergence in early 2020s.

In terms of ground deformation, magma migration and emission process of current Sinabung activity from 2013 is similar to that of Unzendake case in early 1990s when ground inflation and subsequent deflation was detected from campaign data of GNSS (Nishi et al., 1999, JVGR). Chaussard et al. (2013, JGR) detected inflation before the 2010 Sinabung eruption from 2007. Given the volume change amount, magma injection before current Sinabung activity is considered to have started before 2007 (Fig. 3).

Fig. 1. Station map and examples of temporal change in slope distance.

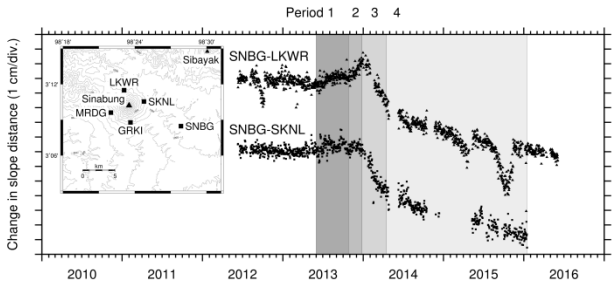

Fig. 2. Schematic description of magma migration process.

Fig. 3. Schematic description of cumulative volume change at Sinabung over time.

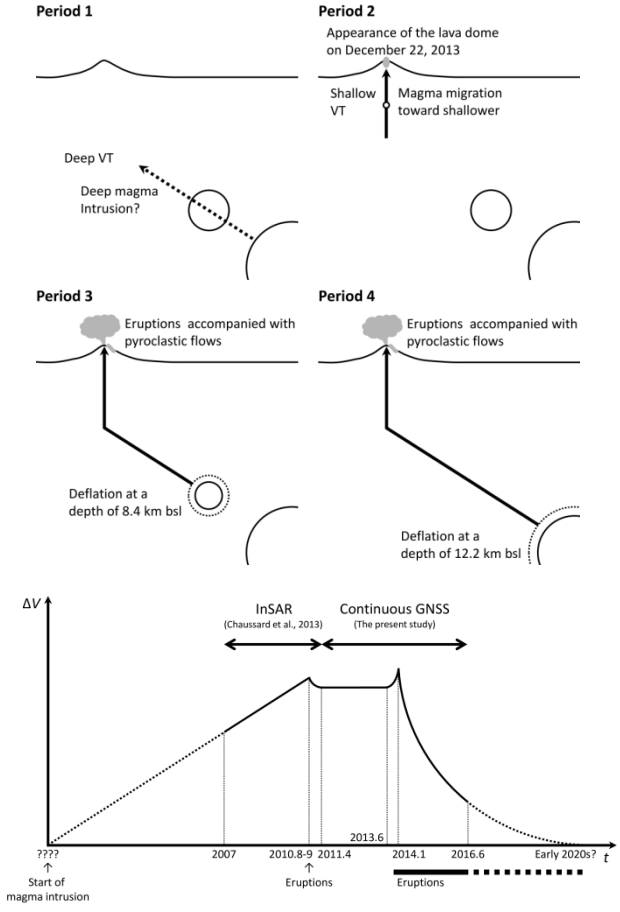

Growth process of the lava dome/flow complex during 2013－2016 at Sinabung Volcano, North Sumatra, Indonesia

○S. Nakada, F. Maeno and N. Hokanishi (Univ. Tokyo), M. Yoshimoto (Fujisan Research Inst.), Y. Suzuki (Waseda Univ.), M. Iguchi and T. Ohkura (Kyoto Univ.), A. Zaennudin, H. Gunawan, and H. Triustuty (CVGHM)

Mount Sinabung, North Sumatra, Indonesia, erupted as its historically first record in 2010 and reactivated since 2013. The eruption was first pheatic and changed into phreatomagmatic before the lava appearance. Andesite lava appeared near the summit crater in late-December 2013, following the summit inflation and elevating seismic activity. Since then, the lava effusion continued, being associated with partial collapses of lava which successively generated pyroclastic density currents (PDCs). The lava complex grew first as a lava dome and developed into a lava flow, which extended up to about 3 km horizontally until mid-2014. When the moving front of the lava complex arrived at the gentler flank, PDC events became rare. Inflation of the upstream side of the lava complex began in mid-2014, being associated with hybrid seismological events plus partial collapses of lava from the top, generating PDC events with longer travel distances. New lobes which appeared repeatedly near the summit disappeared by multiple collapses without growing on steep slopes. The distribution of PDC deposits which extended with time, mostly overlaps with that of the 9 – 10th Century eruption.

The total volume of this eruption reached about 0.13 km^3 as of the end of 2015. The discharge rate of lava was largest in the initial stage (6 m^3/s), and it decreased exponentially with time. Cyclic Vulcanian event began after the summer of 2015 when the discharge rate became low (<1 m^3/s). Since a load of lavas on the vent was not large enough, incomplete degassing of magma in the upper conduit may generate these explosive events instead of intrusion of a solidified plug.

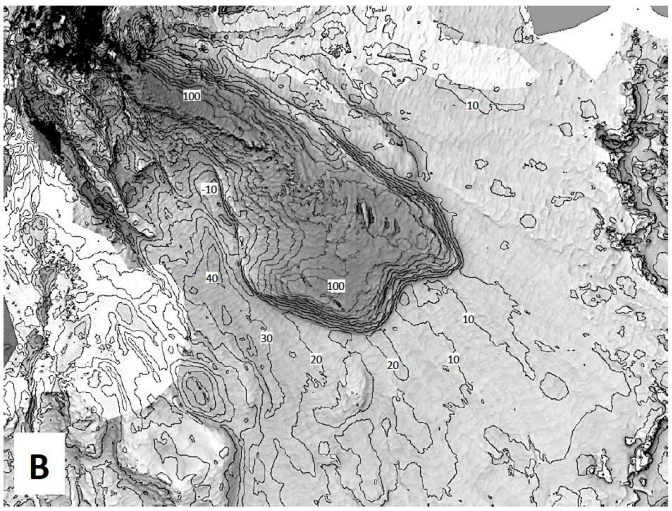

Fig. 1. Relief map of Sinabung Volcano showing the difference in elevation between June 2015 and pre-2010. The unit of contours is in m.

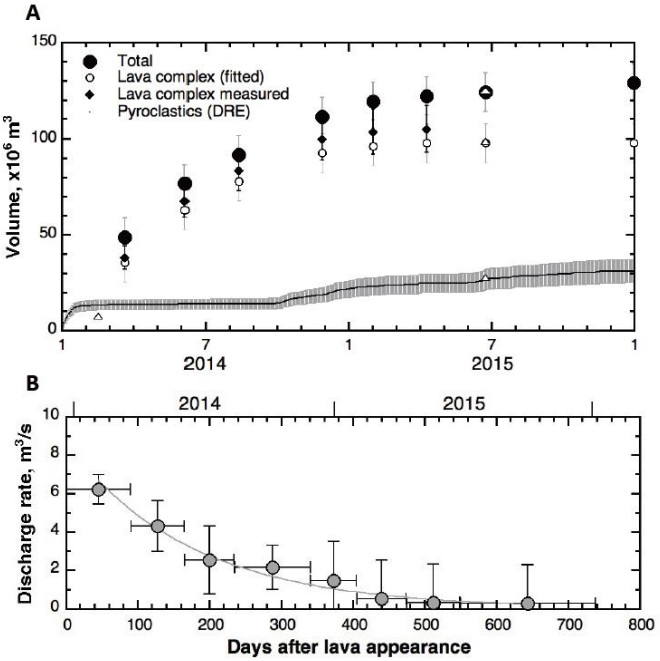

Fig. 2. Temporal volume change of lava complex, pyroclastic density current (PDC) deposits in DRE and the total at Sinabung Volcano (A) and the temporal change in the discharge rate (B).

Historical Development and Recent Status of the Ground Deformation Monitoring at Merapi Volcano, Java Indonesia

I Gusti Made Agung Nandaka, Agus Budi Santoso, Sulistiyani, Ilham Noerdin

Balai Penyelidikan dan Pengembangan Teknologi Kebencanaan Geologi
Jalan Cendana 15 Yogyakarta, Indonesia 55166

Seismic and deformation monitoring are essential methods in identifying symptoms of volcanic activity. The deformation monitoring in Merapi started since the early 1930s when a watertube tiltmeter was installed in the bunker of Babadan Observatory, 4.5 km southwest of Merapi. Ever since, the deformation monitoring of Merapi has evolved along with advances in technology, and in particular due to the cooperation of foreign partners. We will now briefly outline several results of the deformation monitoring conducted in Merapi.

In the early 1980s, in collaboration with the USGS, a geodetic network was built in the summit and around the slope of Merapi for EDM measurement. Most of the benchmarks installed on the slope network still survive to this day. In the early 1990s, electronic tiltmeter using telemetry system was first put into use, in collaboration with the USGS, DPRI/SVO Japan and France. GPS survey began on the 1993 to measure the slope and the summit network. In 1995, a multi parameter station, including a borehole tiltmeter and GPS telemetry, was built in a collaboration coordinated by GFZ Potsdam and VSI Bandung. Study of deformation that measure changes in the body of the volcano using gravimeter were conducted on several occasions in Merapi. Measurement of changes in summit morphology using theodolite was conducted a few months before 2006 eruption. Recently, continuous deformation monitoring network using telemetry system consists of 14 tiltmeter stations, 8 GPS stations in collaboration with SATREPS (Japan) and DoMerapi (France), along with EDM measurement from the observation posts surrounding Merapi.

Applications of modelling using deformation data has managed to locate the source of the pressure, the estimated volume of the magma chamber, as well as patterns and variations of deformation over time prior to the eruption. In general, it appears that the precursory deformation prior to the eruption is quite powerful. The problems occurring in the deformation monitoring of Merapi, among others, is that the methods and techniques applied are not always continuous for a wide variety of reasons (shifting of locations, changes in instruments, etc.). Currently, BPPTKG, which responsible for volcanic activity monitoring in Merapi, is seeking to build a monitoring system independently, by adopting methods and techniques that have been implemented through cooperation with foreign partnerships.

Combination Model of Spherical Source and Block Movement for Asymmetric Ground Deformation Prior to The Eruptions in 2006 and 2010 at Merapi Volcano

Nurnaning Aisyah[1,3], Masato Iguchi[2], Sunarta[3], Yulianto[3], Suparwaka H. [3], Triyono[3], Sopari A. [3], Purwono[3], Alzwar N[3]

[1] Graduate School of Science, Kyoto University
[2] Disaster Prevention Research Institute, Kyoto University
[3] Ministry of Energy and Mineral Resources, Geological Agency, Center For Volcanology and Geological Hazard Mitigation

Ground Deformation

Asymmetric ground deformation prior to the eruptions in 2006 (VEI II) and 2010 (VEI III) at Merapi volcano were detected by Electronic Distance Measurement. Slope distances were measured toward 12 reflectors installed on the flanks from 5 Post Observatories every day. The slope distance shortened 0.03 - 4.4 m for 7 months before eruption 2006 and 0.02 – 3.8 m for 16 months before the 2010 (Figure 1.a, 1.b). All of the CSD (Change of Slope Distance) at S sector were much larger 3.4 – 4.4 m than the other sectors 0.03 – 0.5 m before eruption 2006, and the dominance of CSDs on the S sector 1.1 – 3.8 m to the other sectors 0.02 – 0.06 m. Therefore, we assume that such a large deformation only on the S sector was caused by a block movement and apply Block Movement model to CSDs on the S flank. After remove of the effect of Block Movement on the S flank, Mogi model is applied to the CSDs on the all sectors. CSD data are several periods (Table 1) divide by CSD rate.

Results

Block movement vectors for the first stages (Sept. 2005 to Feb. 2006) before the eruption 2006 is directed to SW, then it moved to SE in second stage (Feb. – Mar. 2006), and this trend continued till the appearance of lava dome (Figure 1.d). The block movement vectors moved to SE constantly from beginning of deformation till the 2010 explosive eruption (Figure 1.e).

A pressure source prior to the eruption in 2006 is located NE of the summit at depth of 0.5 – 2 km. While for eruption in 2010, it is located at deeper 3 – 4 km in NE of summit. Intensity values (K value) of eruption 2006 are shown in Table 1. It reached a peak 4 x 10^6 m^3 in the 1st period. While maximum K value is 46 x 10^6 m^3 (in the last period before eruption 2010). The values indicate volume of magma stored before the eruptions. The magma volume prior to the eruption 2010 is larger than the eruption 2006 and the difference may be related to the difference in VEI between the eruptions.

Table 1.

Eruptions	Periods	K value (m^3)
Eruption 2006	September 2005 to 12 February 2006	4 x 10^6
	12 February to 8 March 2006	0.8 x 10^6
	8 to 29 March 2006	3 x 10^6
	29 March to 12 April 2006	2 x 10^6
	12 to 18 April 2006	2 x 10^6
	18 to 20 April 2006	0.6 x 10^6
	20 to 26 April 2010	0.4 x 10^6
Eruption 2010	April to December 2009	7 x 10^6
	January to September 2010	4 x 10^6
	2 to 24 September 2010	9 x 10^6
	24 September to 5 October 2010	29 x 10^6
	5 to 15 October 2010	14 x 10^6
	15 to 20 October 2010	44 x 10^6
	20 to 21 October 2010	2 x 10^6
	21 to 23 October 2010	29 x 10^6
	23 to 24 October 2010	32 x 10^6
	24 to 25 October 2010	9 x 10^6
	25 to 26 October 2010	46 x 10^6

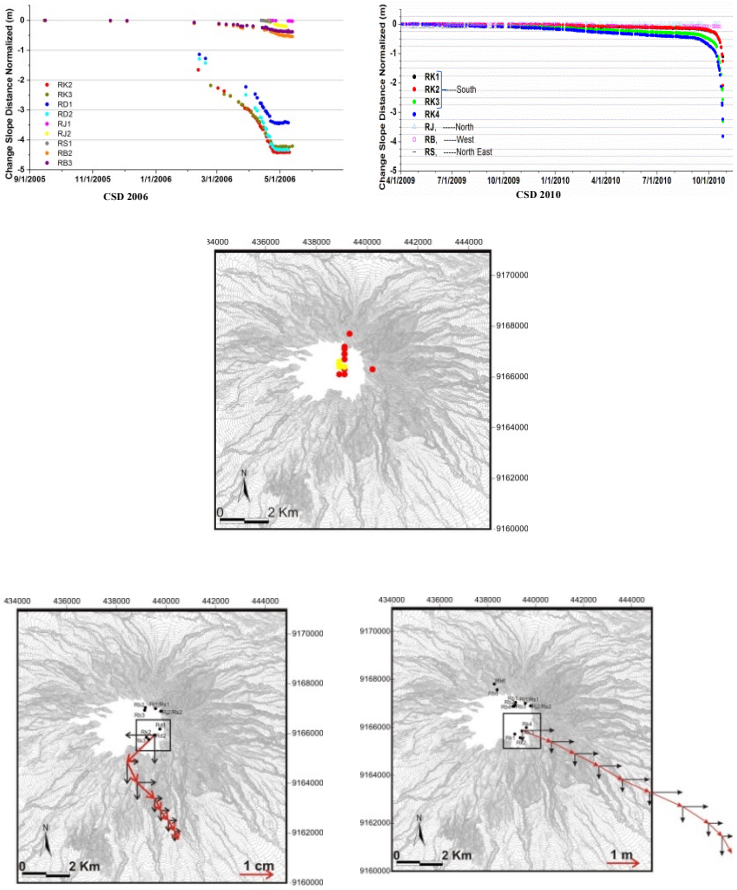

Figure 1. CSD eruption 2006 and 2010 (a,b); location of the pressure source (c) in 2006 (yellow triangle) and 2010 (red triangle); block movement vectors before 2006 (d) and before 2010 (e).

Volume of pyroclastic flow forecasted by precursory seismicity of Merapi volcano

○M Iguchi, H Nakamichi (Kyoto U.), K Miyamoto, M Shimomura (U. Tsukuba),
IGM Agung Nandaka, Agus Budi Santoso, Sulistiyani, N Aisyah (BPPTKG)

Pyroclastic flows frequently occurred at Merapi volcano, Central Java. Eruption from October to November 2010 ejected pyroclastic material $1.3\times10^8 m^3$ and pyroclastic flow reached a distance17 km from the summit. Volcanic earthquakes at Merapi volcano are classified into volcano-tectonic type (VA; >2km deep, VB; <2km) and MP, LF and rock-fall. Prior to the 2010 eruption, seismicity of VT and MP increased gradually from the middle of September and accelerated in October. Seismic energy of the precursory activity was estimated to be 1×10^{11}J. On the other hand, seismic energy prior to 1997, 1998, 2001 and 2006 eruptions were only $2\sim3\times10^{10}$J and these eruptions produced pyroclastic flows with the volumes of $2\text{-}8\times10^6 m^3$. This suggests a relation with precursory seismicity and volume of following pyroclastic flow at Merapi.

White and McCausland (2016, JVGR) compiled precursory seismicity prior to representative eruptions in the world. Examining plots between precursory seismicity versus VEI based on Table 1 of White and McCausland (2016), the volumes of pyroclastic material produced by the eruptions from 1997 to 2010 are located at upper limit of VEI as related with precursory seismicity. The upper limit is approximated as;

$$\mathrm{Log}_{10}V=2\mathrm{Log}_{10}E_s-13.7 \qquad (1)$$

where V is upper limit of volume in m^3 and E_s is precursory seismic energy in Joule.

BPPTKG responsible to monitor Merapi volcano compiles daily seismic energy since 1990. It is possible to forecast volume of pyroclastic flow from cumulative seismic energy based on eq (1). Potential volumes are evaluated day-by-day from cumulative seismic energy by shifting window of 365 days. Seismic energy is sum of VA, VB and MP types following BPPTKG's conventional evaluation. Results are shown in Fig. 1. Potential volume increased according to increase in seismicity. Potential volumes are a little bit larger than actual volume of pyroclastic material. The difference could be reduced by adjusting parameters in Eq. (1). Fig. 2 shows an enlargement for the 2010 eruption. Potential volume increased, well corresponding to upgrading alert level. Distance and thickness of pyroclastic flow deposit can be evaluated day-by-day by putting the daily potential volume into simulator of pyroclastic flow.

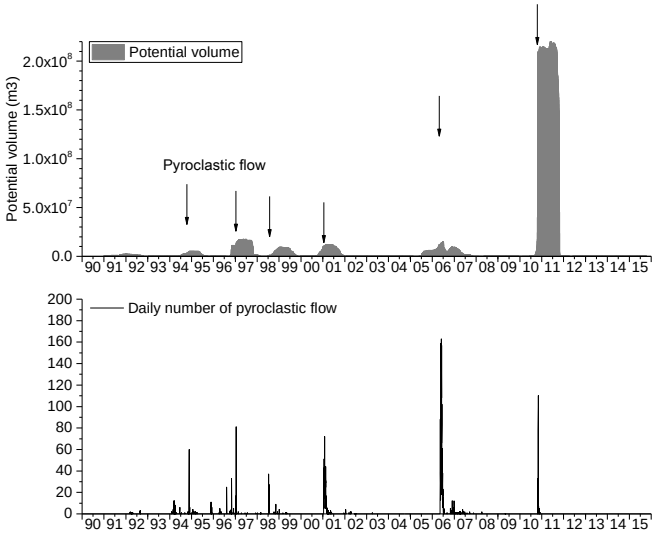

Fig. 1 Daily evaluation of potential volume of pyroclastic material during the period from 1990 to 2015.

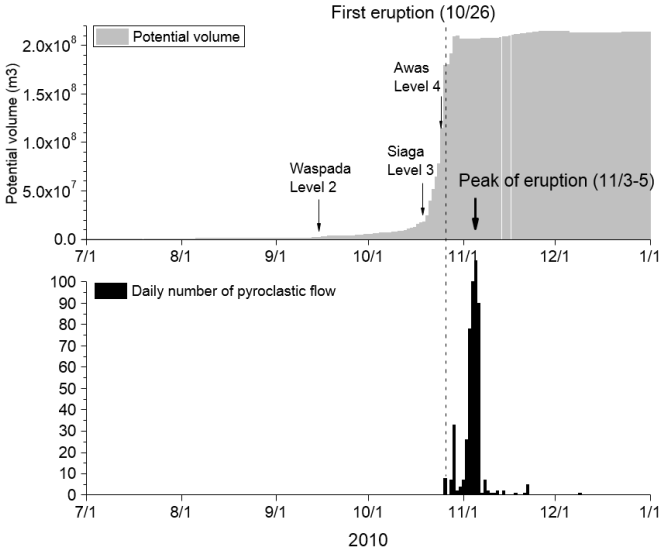

Fig. 2 Daily evaluation of potential volume of pyroclastic material during the period from July 2010 to December 2010. High-level potential volume after the eruption is due to long-term (365 days) window analysis.

Velocity variations associated with the large 2010 eruption of Merapi volcan, Java, retrieved from seismic multiplets and ambient noise cross-correlation.

Agus Budi-Santoso[a,b], Philippe Lesage[b]

[a] Badan Geologi, Jalan Diponegoro No. 57, 40122 Bandung, Indonesia

[b] ISTerre, CNRS, Université Savoie Mont Blanc, 73376 Le Bourget du Lac Cedex, France

Abstract

We present a study of the seismic velocity variations that occurred in the structure before the large 2010 eruption of Merapi volcano. For the first time to our knowledge, the technique of Coda Wave Interferometry is applied to both families of similar events (multiplets) and to correlation functions of seismic noise (NCF). About half of the seismic events recorded at the summit stations belong to one of the ten multiplets identified, including 120 similar events that occurred in the last 20 hours preceding the eruption onset. Daily noise cross-correlation functions (NCF) were calculated for the six pairs of short-period stations available. Using the stretching method, we estimate time series of apparent velocity variation (AVV) for each multiplet and each pair of stations. No significant velocity change is detected until September 2010. From 10 October to the beginning of the eruption on 26 October, a complex pattern of AVV is observed with amplitude of up to ± 1.5 %. Velocity decrease is first observed from families of deep events and then from shallow earthquakes. In the same period, AVV with different signs and chronologies are estimated from NCF calculated for the various station pairs. The location in the horizontal plane of the velocity perturbations related with the AVV obtained from NCF is estimated by using an approach based on the radiative transfer approximation. Although their spatial resolution are limited, the resulting maps display velocity decrease in the upper part of the edifice in the period 12-25 October. After the eruption onset, the pattern of velocity perturbations is significantly modified with respect to the previous one. We interpret these velocity variations in the framework of a scenario of magmatic intrusion that integrates most observations. The perturbation of the stress field associated with the magma migration can induce both decrease and increase of the seismic velocity of rocks. Thus the detected apparent velocity variations can be considered as precursors of volcanic eruptions in andesitic volcanoes, without taking their sign into account.

Volcanic earthquake activity analysis and eruption imminent evaluation system using seismic data

○Haruhisa Nakamichi and Masato Iguchi

(Sakurajima Volcano Research Center, Disaster Prevention Research Institute, Kyoto University)

Since seismic observation is a basic volcano monitoring tool, every volcano observatory has at least one short-period seismometer at a target volcano. Every volcano observatory routinely counts number of earthquakes and their amplitudes. It is well known that magma intrusions are frequently associated with volcano-tectonic (VT) earthquakes. VT swarm has been interpreted as a brittle response of the volcanic rock to transient changes in stress transferred by magmatic fluid movements or material damage of the volcanic rock through fracture growth and fault movement. Many types of volcanic eruptions and associated phenomena are preceded by increases in the rate and amplitude of earthquakes, and these signals are key pieces of information used in volcano monitoring.

Digital observation networks have been constructed at Guntur, Galunggung, Merapi, Semeru, and Kelud volcanoes in Java, in the period from January to September 2015 by CVGHM and Kyoto University under the SATREPS project "Integrated Study on Mitigation of Multimodal Disasters Cause by Ejection of Volcanic Products". The network at each volcano consists of two short-period three-components seismic stations, three or four GNSS stations, and one tiltmeter station, their data are transmitted via 5.8GHz WiFi to the observatory (POS), and continuously stored and processed on windows PCs at POS (Fig. 1).

The WIN(A1)-formatted seismic data are stored in disk and transmitted to another PCs by the software Arga Lite, and also analyzed by new software, consisting of two parts of applications "volcanic EarthQuakes Analysis (EQA)" and "Eruption Imminent Evaluation (EIE)". The both applications run on the environment of Windows 7 or 8.1, .Net Framework 4.5 or later, Java 1.7 or later, 2TB or larger HDD, and 4GB or larger physical memory.

The EQA receives WIN data packets on a port of the shared memory, and calculates maximum and RMS amplitudes at one-minute time windows from raw and filtered seismic waves, and make running-spectrum and also detects and classifies seismic events as A(VT), B(low-frequency), non-volcanic, and explosion earthquakes. The EQA also has a function to estimate amounts of ash by using the empirical equation proposed by Iguchi (2016) as follows:

$$W_{seis} = \alpha A + \gamma \qquad (1)$$

where W_{seis} is ash weight (unit in tons), A is seismic amplitude (unit in m/s), α and γ are constants. α is from several tens to several hundreds, which is determined by monthly sum of seismic amplitudes and measured weights of ash.

The EIE uses the RMS seismic amplitudes at each minute obtained by the EQA to calculate seismic energy. To calculate the energy, geometrical spreading, hypocentral distance, attenuation of seismic waves, propagation speed of waves, and density of medium are considered. The EIE has a trigger function using four thresholds of seismic energy level. When the trigger is on, the EIE fit cumulative seismic energies to the logarithm function as follows:

$$f(t) = a\log(1 + bt) + c \qquad (2)$$

where a, b and c are constants. The predicted time of eruption t_f is expressed by $t_f = -1/b$.

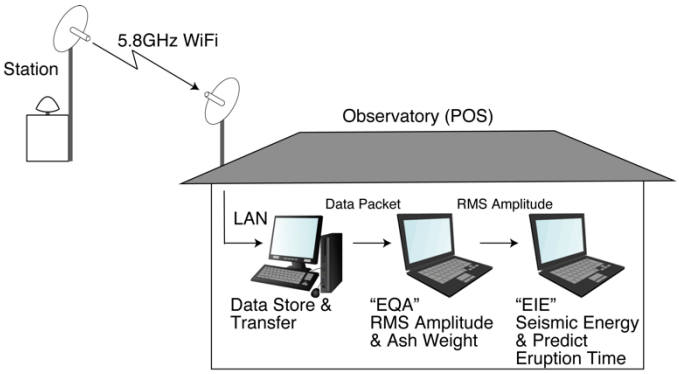

Fig. 1 Seismic data flow from stations to PCs. EQA and EIE applications are running on the PCs.

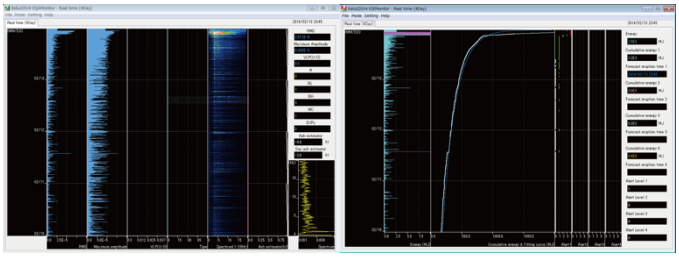

Fig. 2 Screen-shot of EQA (left) and EIE (right) applications.

Rainfall characteristics on the southern flank of Mt. Merapi in Indonesia

○Y Gonda, S Shimbo (Niigata U.), S Miyata, M Fujita, D Tsutsumi (Kyoto U.)

Temporal and spatial characteristics of rainfall are essential information to predict rainfall-induced sediment disasters such as lahars and slope failures. Around Mt. Merapi, ground rain gauge network was developed in November 1984 to operate the early warning system for lahar hazards (Shuin et al., 1995) and 10 min-rainfall observation has been continuing since then. However, localized torrential rains specific to tropical regions frequently occur there and their rainfall areas are narrow. Therefore, it seems that rainfall events, which induce lahars, cannot be detected enough efficiently by the ground rain gauge network. To improve efficiency of the early warning system for lahar hazards, temporal and spatial charanteristisc of rainfall around Mt. Merapi should be studied.

Temporal and spatial characteristics of rainfall there were studied in early 1990 by Shuin et al. (1995) using groud rain gauge network and a C-band radar. Howeve some local people say that rainfall characteristics have changed recently. Under the SATREPS project, a X-band MP radar rain gauge was installed on the south frank of Mt. Merapi and its operation started in 2015(Oishi, 2015). The X-band MP radar rain gauge provides us rainfall information with higher spatial resolution and higher temporal resolution then ground rain gauge network and former C-band radar.

In this study, rainfall characteristics on the south-southwestern in recent years were analyzed using rainfall data monitored by ground rain gauges at Gunung Maron, Babadan and Plawangan and spatial correlation of rainfall was analayzed using rainfall data monitored by ground rain gauges at BE-D4 and Turge and the X-band MP radar rain gauge (Table 1, Fig. 1).

Rainfall characteristics at Babadan, Plawangan, Gunung Maron in 2012, such as frequency on rainfall intensity, number of rainfall, average of net storm rainfall, relationship between maximum rainfall and net storm rainfall, were compared with those in 1990. However, there aren't significant differences between them. Change in rainfall characteristics at Gunung Maron over year was statistical tested using variance analysis. As a result, no significant secular change in rainfall characteristics was recognized (Fig. 2). These results suggest that there is no significant change between in recent years and in 1990's,

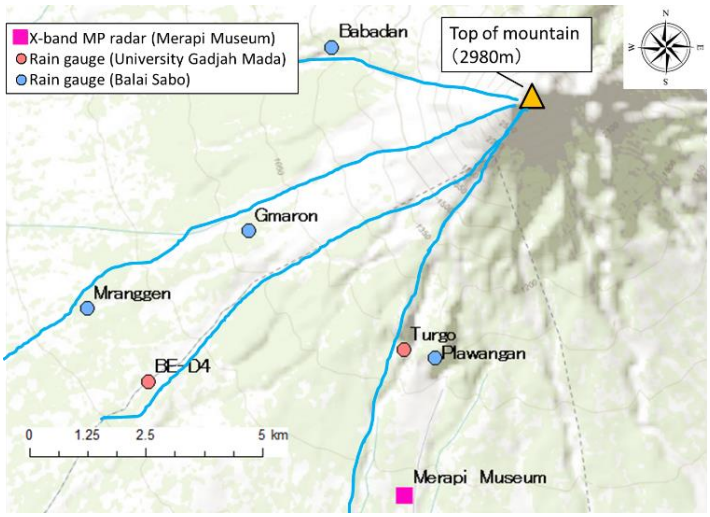

Fig. 1 Location of rivers around Mt. Merapi and allocation of rain gauges used in this study

Table 1 Rainfall data used in analysis

Location	Altitude	River Basin	Equipment /Recording interval	Analysis period
Gunung Maron	951m	Putih	Rain gauge /10[min]	Oct.1984-Sep.1992 Jan.1996-Dec.1998 Jan.2004-Dec.2005 Jan.2012-May.2013
Babadan	1210m	Pabelan		Jan.2012-May.2013
Plawangan	1103m	Boyong		Jan.2012-May.2013
BE-D4 sabo dam	663m	Krasak	Rain gauge / 3[min]	Nov.2015-Jan.2016
Turgo	987m	Boyong		
Merapi Museum	700m	Boyong	X-Band MP radar / 2[min]	

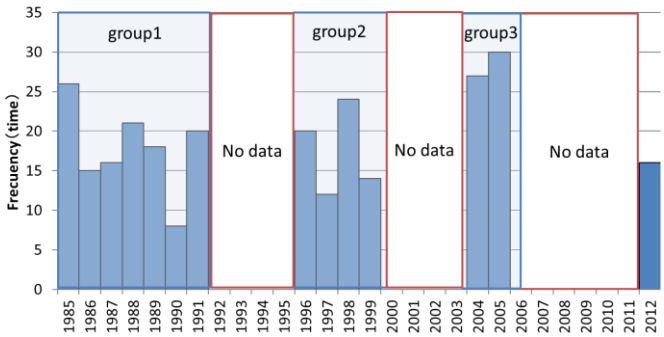

Fig. 2 Frequency of rainfall events with maximum intensity over 30(mm/h) at Gunung Maron

though year to year variability of rainfall characteristics seems to be large. Spatial correlations of 10 minutes' rainfall were calculated along the east-west line and the north-south line through Turgo (Figs. 3 and 4).

Spatial correlations decrease with the distance from Turgo. However, decrease rates per distance were different among the direction. Shuin et al. (1995) defined the area of which spatial correlations ≥ 0.7 is spatial realm covered by a rain gauge at a given spot in their study conducted around Mt. Merapi. According to their definition, spatial realms at Turgo are 3km along east-west direction and 1-1.5km along the north-south direction. These results suggest that rainfall area at Turgo tends to be anisotropic and its length along north-south direction tends to be shorter than east-west direction.

In order to confirm validity of the spatial realm covered by a rain gauge estimated above, time series of 10 minutes' rainfall data at Turgo, 0.5km downstream location(0.5ds) and 1.0km downstream location(1.0ds) from Turgo were extracted from the rainfall data by X-Band MP radar rain gauge. A drainage area of approximately 9km^2, which contain Turgo, 0.5ds and 1.0ds was drawn and series of the drainage area average 10 minutes' rainfall data was calculated from the rainfall data by X-Band MP radar rain gauge.

Fig. 5 shows an example of Hyetograph of these rainfall data. Compared among hyetographs at Turgo, 0.5ds and 1.0ds and that drawn with the drainage area average rainfall, shapes of hyetographs and values of peak rainfall were deferent each other. Especially shape of hyetograph at 1.0ds is clearly different from others. The hyetograph at 1.0ds contains only one peak though other hyetograph contain two peaks. Total amount of rainfall during the time period shown on the Fig. 5 at Turgo, 0.5ds and 1.0ds are 6.8mm, 5.1mm, and 3.9mm respectively, while that of the drainage area average rainfall was 8.8mm. Total amount of rainfall at 1.0ds about a half as much as drainage area average rainfall. These results indicate that the rain gauge installed at Turgo represents rainfall condition only within the spatial realm.

In order to predict occurrence of lahar effectively, it is very important to collect rainfall information accurately, especially short-term rainfall such as 10 minutes' rainfall, at upper reach of the river, where lahar is initiated. Under the existing lahar warning system at Mt. Merapi, the risk of the lahar occurrence is judged by the rainfall information collected the ground rain gauges at an altitude of 1000m installed each other at approximately 4 - 5 km intervals. The results of spatial correlation of 10 minutes' rainfall around Turgo imply that the ground rain gauges network cannot detect occurrence of rainfall events effectively.

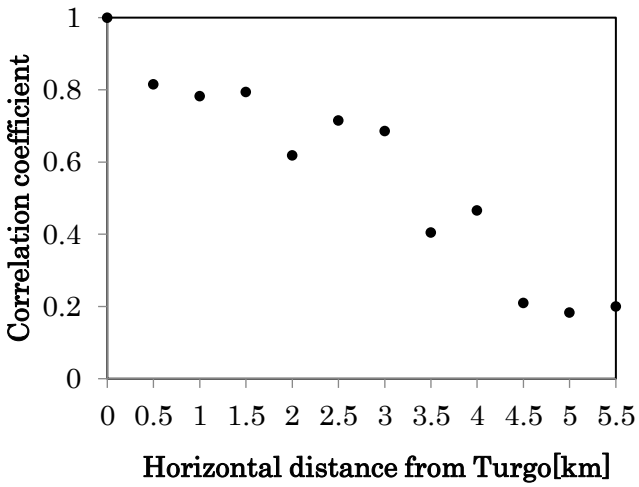

Fig. 3 Spatial correlation of 10 minutes' rainfall monitored by X-Band MP radar along the east-west line from Turgo to BE-D1 sabo dam.

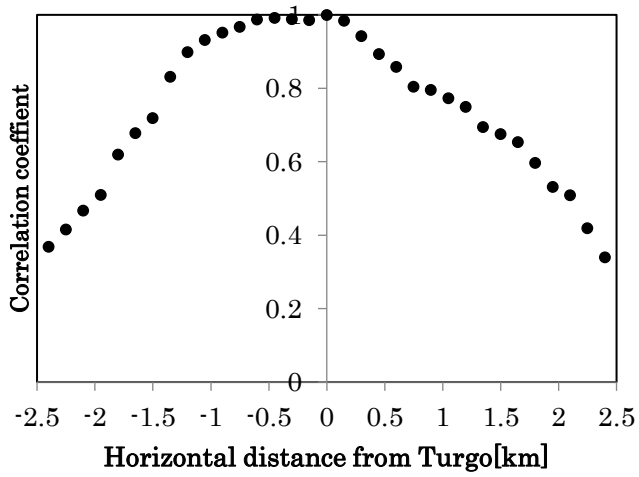

Fig. 4 Spatial correlation of 10 minutes' rainfall monitored by X-Band MP radar along the North-south line through Turgo.

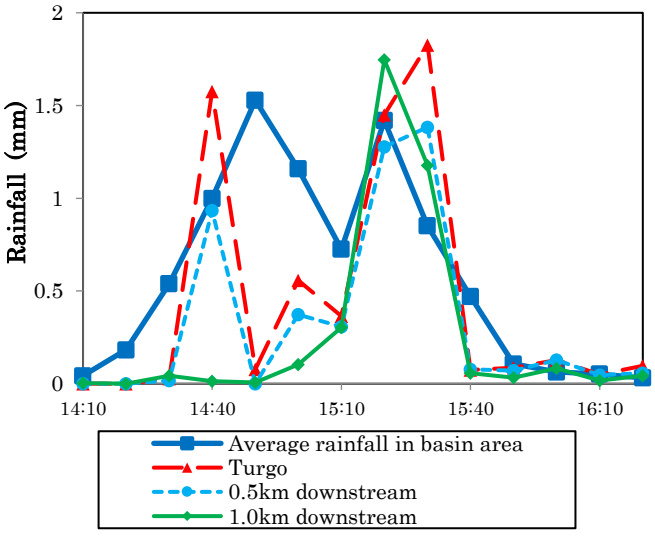

Fig. 5 Comparison of Hyetograph around Turgo

Radar Information at. Mt. Merapi Area and Various Water & Sediment-related Disasters - Case of 18 June 2016

○Rachmad Jayadi, Hanggar Ganara Mawandha, Ani Hairani (Gadjah Mada U.), Sutikno (Balai Sabo)

Mt. Merapi is a very active volcano in Indonesia which potentially creates pyroclastic flow as its primary disaster and lahar flow as the secondary disaster. Those disasters are very likely to cause major damage and even casualties. Moreover, the natural disasters are triggered by high precipitation intensity in which the generated runoff are causing the river flow to carries the sediment materials.

The X-band Multi Parameter Radar installed on the rooftop of Volcano Merapi Museum building has been operated as one of SATREPS project program that very beneficial to increase the mitigation capacities of those disasters in the slope areas of Mt. Merapi, especially in the south area which is a dense urban areas. The radar can measure and summarized meteorology data, precipitation data, and data of volcanic ashes due to eruption.

This paper delivers the simple comparison results of radar estimated and rain gauge measured precipitation in several locations. One of the example for the collected data was during extreme precipitation event on June 18th, 2016 that caused flash flood and landslides in 6 villages of Purworejo district, Central Java, around 60 km away from Yogyakarta. The disasters bring about hundreds of damaged houses, 30 casualties, and 13 people missing (Metrotvnews.com, 20 June 2016). Fig. 1 shows the condition in one of the landslides location. The 5 hours measured precipitation in the most severe area is Bogowonto watershed with 328 mm in Kedungputri and 285 m in Kaligesing.

The recorded radar precipitation and measured on three rain gauges in south slope Mt. Merapi, i.e. BE-D4, Sukorini and Turgo were not showing a high intensity. Fig. 2 presents those comparisons of instantaneous rainfall intensity measured by the radar and rain gauge in Sukorini. The comparison of 30 minutes rainfall intensity is also processed for the precipitation event on 24 September 2016, as shown in Fig. 3. The ratio between the amount of precipitation measured by rain gauge and radar (G/R ratio) in 5 rain gauge locations can be seen on Fig. 4. The results of those two events show that the radar rainfall are not quite similar to those measured by rain gauge.

Further research are necessary to increase accuracy of precipitation data base of MSD system simulator for providing a more reliable lahar flood early warning in the slopes area of Mt. Merapi.

Fig. 1 Land slide on 18 June 2016 in Purworejo.

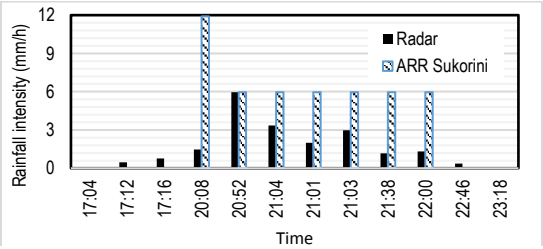

Fig. 2 Comparison of instantaneous rainfall intensity in Sukorini rain gauge on 18 June 2016.

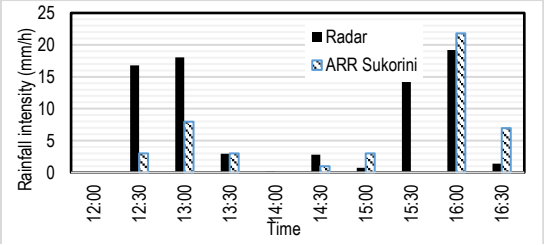

Fig. 3 Comparison of 30 minutes rainfall intensity in Sukorini on 24 September 2016.

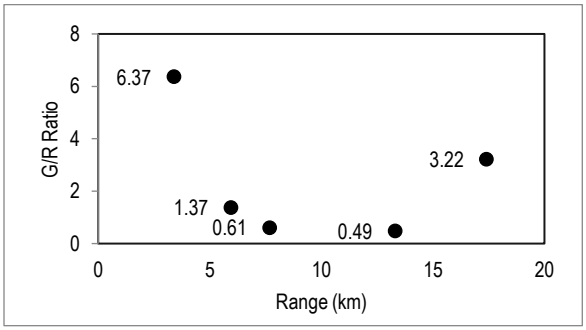

Fig. 4. G/R ratio trend to distance of 5 rain gauge locations on 24 September 2016.

Temporal change of infiltration characteristics of volcanic ash layer and its effect on rainfall-runoff processes

Shusuke Miyata (Kyoto Univ.), Heba Ahemad (Kyoto Univ.), Masaharu Fujita (Kyoto Univ.), Hirofumi Tsujimoto (Kyoto Univ.), Takuji Teratani (Japan Weather Association)

Volcano eruptions yield volcanic ash on mountain slopes, which can enhance runoff of water and sediment. However, changes of hydrological characteristics of the newly supplied volcanic ash are little understood. To evaluate temporal change of runoff and infiltration characteristics on slopes covered with volcanic ash, we conducted an in-situ experiment in which a containers filled with volcanic ash and soil was exposed to rainfall and overland flow was measured in Sakurajima, Kagoshima, southern Japan. In the containers, a volcanic ash layers of 1-cm thickness was laid on subsurface gravel and soil layers. No overland flows were observed when rainfall intensity was less than 0.5 mm/5min. Runoff ratio of overland flow tended to increase with cumulative rainfall (Fig. 1). These experimental results suggested that compaction or disturbance of the surface ash layer contributed the increase of runoff ratio. Based on these experimental results, we improved a rainfall-runoff model for catchments covered by ash layers.

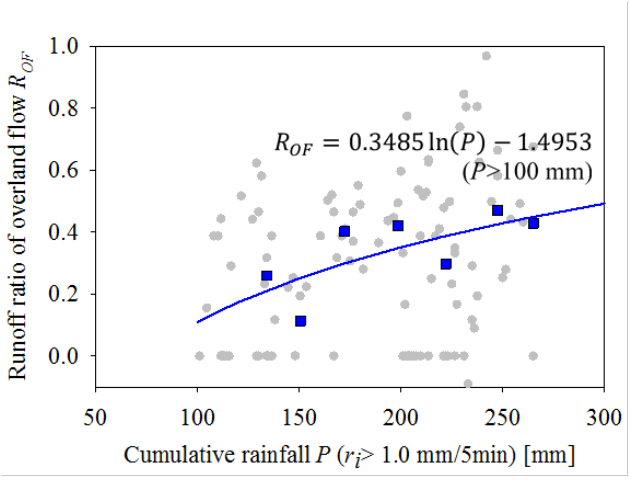

Fig. 1 Relationship between overland flow runoff ratio and cumulative rainfall in an in-situ experiment.

Real-time lahar hazard map generation using X-MP radar forecast products in Merapi volcano

○R I Hapsari (State Polytechnic of Malang), S Oishi, M Syarifuddin (Kobe U.),

Debris flow disaster accompanying the volcanic eruption is noticed as the most serious secondary impact of volcanic disaster. The sediment-related disaster is highly triggered by rainfall. X-band weather radars have been extensively used in recent hydrological disaster researches and operations. In this study, debris flow or lahar disaster mitigation system by utilizing the high-resolution nowcasting products from X-band multiparameter compact (X-MP) is presented. The study area is the rivers on Mount Merapi which is historically one of the most active volcanoes in Indonesia. With its high volcanic activities, the rivers in this area have been affected greatly by the ejection of volcanic material.

Extrapolation model which has been the mainstream of rainfall nowcasting until recently is used to predict the rain echo motion observed by X-MP radar with lead time of 2 to 5 hours (Shiiba et al., 1984). The lahar hazard map information is developed by evaluating the maximum 1-hour rainfall in one event (mm/h) and the working rainfall in 7-days before the maximum 1-hour rainfall (mm/h) (MLIT, 2004) obtained from X-MP radar nowcasting in grid mesh units. The rainfall critical line from past empirical studies (Mananoma and Wardoyo, 2009; Sutikno et al., 2013) for each river basins is used to categorize the high and medium hazard level of rain-triggered lahar. By using this map, the vulnerable river to lahar flow can be predicted in real-time scheme. In order to provide more specific warning information in localized scale, snake line or temporal variation of real-time hourly and working rainfall from radar nowcasting products is drawn in the rainfall critical line diagram to judge the timing debris flow occurrence.

This scheme is reviewed through the application in two river basins, Putih River and Gendol River. Heavy rainfall occurred on February 17, 2016 is taken as a case study. During this event, Pabelan and Gendol Rivers were hit by debris flow. The hazardous area information observed by radar observation in this event are confirmed with condition of lahar occurrences in these rivers on that day. The results show the conformity of the real case and the potential lahar disaster given by the hazard map (Fig. 1).

The extrapolation model is run with the initial time of 14:40, 14:50, and 15:00 LST. The rain spatial distribution at 1 hour lead-time or 16.00 LST and its hazard map product are shown in Fig. 2 and Fig. 3. Compared with the observation, the rain prediction shows the uncertainty. This prediction error may be sourced from the small scale of the event, in addition to the prediction model itself. Regardless of this shortcoming, the system could help to show the potential of the debris flow disaster in the region. In the future study, the ensemble rain prediction is introduced aiming to gain the knowledge of inherent uncertainties.

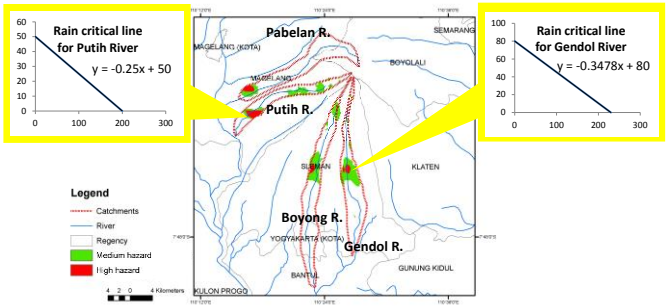

Fig. 1 Hazard level of February 17, 2016 event in 4 basins; rainfall critical line for Putih and Gendol River.

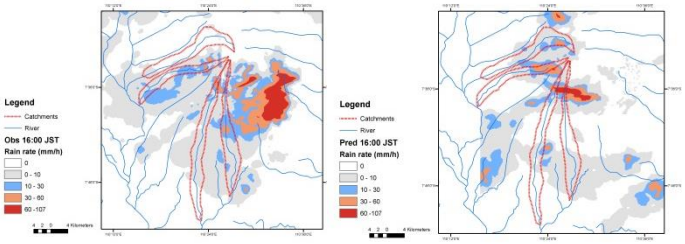

Fig. 2 Rain observation (left) and prediction (right).

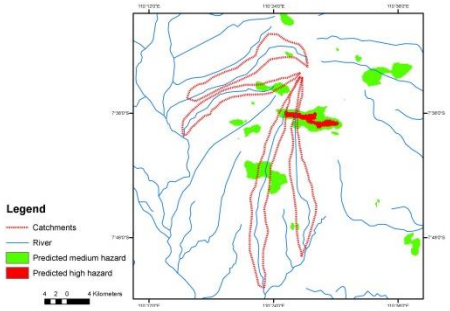

Fig. 3 Hazard map from predicted rainfall by X-MP radar with 1-hr lead time prediction at 16:00 JST.

A Dynamic Hazard Level Assessment of Lahar in Mount Merapi

○M Syarifuddin, S Oishi (Kobe U.), RI Hapsari (State Polytechnic of Malang),
D Legono (Gadjah Mada U.), M Iguchi (Kyoto U.)

This research combines qualitative and quantitative methods to develop a new technique for dynamic lahar hazard level assessment in Mount Merapi of Indonesia. Qualitatitve method was done by analyzing the susceptibility map of sub-basins relying on Digital Elevation Model (DEM) only and quantitative method was done by the numerical model of debris flow to simulate real lahar event and its impact on the lahar hazard occurrence. The developed framework is also compared to analysis that relying only on qualitative method.

Four parameters (maximum elevation, basin orientation, Melton Ratio and average slope) were extracted from 316 sub-basins in Mt. Merapi. K-means cluster analysis was done for those parameters resulted in 31 sub-basins were classified as high susceptible (S1) and 91 sub-basins are moderate susceptible (S2). Three classes of rainfall were also classified by using dummy regression to analyze the historical lahar events and raingauge data (qualitative analysis), while numerical model of debris flow was used to classify the rainfall based on the flow concentration in each sub-basin (quantitative analysis). Last, fuzzy logic analysis was done to determine the combination of sub-basins susceptibility and rainfall condition (Fig. 1).

The framework was applied into a rainfall events that lead to lahar occurrence on 17 Feb. 2016 (Fig. 2). The qualitative method resulted in most of the sub-basins in the summit of Mt. Merapi to have high possibility of lahar occurrence (C3), while the dynamic method (combination of qualitative and quantitative) indicates only five sub-basins in Putih Catchment, Gendol Cathment and Woro catchment are classified to be in high lahar hazard class (Fig. 3a and Fig. 3b). Although it still gives one false alarm but it shows similarity to real condition.

In general the dynamic method gives better understanding on regional scale of Early Warning System (EWS) and is able to represent the dynamic aspects of Mt. Merapi spatially and temporally.

		Sub-basin Susceptibility		
		Low	Moderate	High
Rainfall Situation	Weak	Low (C1)	Low (C1)	Low (C1)
	Moderate	Low (C1)	Moderate (C2)	High (C3)
	Ciritical	Moderate (C2)	High (C3)	High (C3)

Fig. 1 The matrix rule on lahar hazard assessment by combining rainfall situation and sub-basin susceptibility

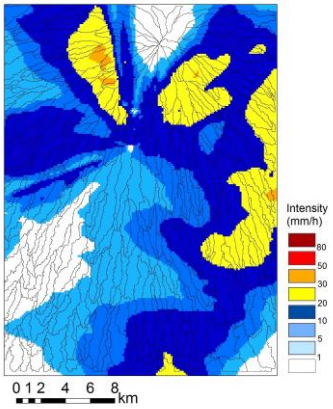

Fig. 2 Average rainfall intensity in the studies area at 15:40-17:40

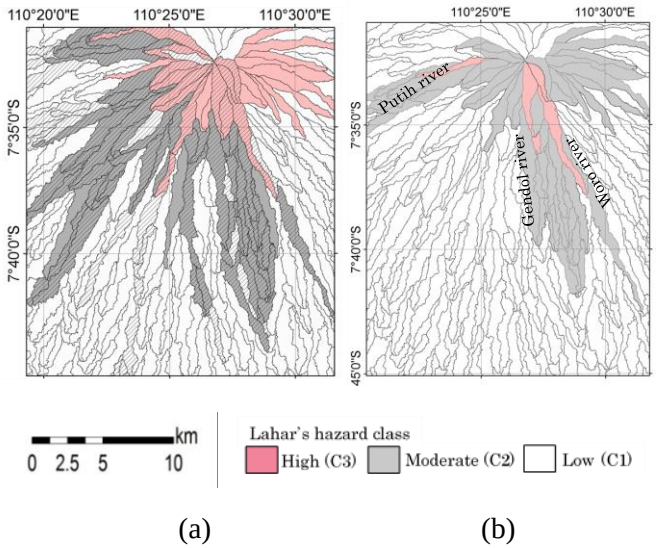

(a) (b)

Fig. 3 Lahar hazard maps generated by qualitative method (a) and dynamic method (b)

An Integration of monitoring data analyis for volcanic hazard assessment

Gede Suantika (CVGHM)

The current strategy for volcanic hazard assessment in Indonesia is by conduct six main activities which are essentially instrumental monitoring, volcanic hazard mapping, volcanic hazard modeling, probabilistic forecast (event tree), technical recommendation and information dissemination related to stake holders. The presentation focus on integration aspect of monitoring data analysis at Sinabung, Kelud and Guntur volcanoes which is also under the SATREPS volcano project target.

Sinabung Volcano is located in the province of North Sumatra, 80 km to the west of the provincial capital, Medan, or 40 km to northwest of Lake Toba. Sinabung Volcano is a stratovolcano with several summit vent/crater, steep flanks features and radial symmetry as as a result from local accumulation of erupted products. The erupted products consists of a series of lava flows, pyroclastic flow deposits, and lava dome complex at the summital area. Sinabung Volcano had no recorded historical eruption, in Indonesian volcanoes classification therefore Sinabung Volcano was classified as B-type, it means that has not erupted in at least 400 years. However since August 29, Center for Volcanology and Geological Hazard Mitigation (CVGHM) monitor the volcano continuously from temporary Sinabung Volcano Observatory after the 29 August 2010 phreatic eruption and CVGHM had been upgraded Sinabung volcano classification from B-type to A-type and raised its level status to Level IV (4 for 4). In that eruption the active vent spewed a 1500 meters ash column. After the 2010 short live eruption persistent fumarolic emissions continued for almost 3 year, before a new eruption began on 15 September 2013. This eruption continues to the present. In October 2010, CVGHM in collaboration with the Disaster of Kyoto University added 6 temporary seismic stations in order to increase the coverage surrounding tectonic faults and Sibayak volcano and also four continuous GPS stations in February 2011. The ongoing eruption is divided into 5 major phases: 1) phreatomagmatic phase (July 2013 – 18 December 2013); 2) first dome and collapse phase with pyroclastic flows/PF (block-and-ash flows and related surges) to south (18 December 2013 – 10 January 2014); 3) lava-flow and collapse phase (10 January 2014 – mid-September 2014); 4) second lava dome and collapse phase with PF to south (mid-September 2014 – July 2015); 5) lava dome collapse and ash explosion phase with PF to southeast and east (August 2015 - present). The volcanic hazard map of Sinabung volcano has been revised three times with considering the

probability of ash eruption and phyroclastic flows.

Kelud volcano is a strato volcano, located in three regencies of Kediri, Blitar and Malang, East Java Province, Indonesia. Kelud's eruptions are characterized by explosive eruption (magmatic) which eject materials with size from ash-sized to rocks and pyroclastic flows. The last eruption of Kelud volcano was on 13 February 2014. It was seven years after extrusion of lava dome in the crater lake in 2007.The eruption was determined to be a VEI 3-4 eruption and destroyed the 2007 lava dome. The eruption caused the monitoring system of Kelud volcano destroyed. Only one seismic station far from the crater, which still works after the eruption. Within SATREPS cooperation project, in 2014 there are 4 continuous GPS which has been installed and also some additional 3-component seismometers. In 2015 X-band MP radar was installed at Selorejo (20 km to east of Kelud edifice) for rain-ash cloud monitoring which dedicated to the lahar hazard mitigation. As for the volcanic hazard map of Kelud volcano has been revised last year with considering the probability of eruption and phyroclastic flow and lahar simulation.

Guntur volcano is a stratovolcano in western Java which its last eruption was in 1847. For over more than at least 20 years ago the seismic activity of Guntur volcano is always relatively high however the Guntur's activity level status is always almost in the lowest level. In the past the Guntur's activity level status had been upgraded from Level I into Level II in 1997 and in 2013. Indonesia-Japan cooperation in Guntur has been a long time since the 1990s in which the monitoring system G. Guntur grown with the addition of seismic and deformation instruments. In SATREPS cooperation project some seismic equipment have installed including 3- components seismometers and tiltmeters, while the installation of continuous GPS were done under the previous period of the SATREPS cooperation project. As for the volcanic hazard map of Guntur volcano has been revised last year with considering the probability of eruption and phyroclastic flow and ash fall simulation, which will be affect the nearest prone areas in the future.

Examination of characteristics of tilt records associated with vulcanian eruptions at Sakurajima volcano

○T Nishimura and R Nakajima (Tohoku Univ.)

Ground deformatioin at volcanoes can capture the spatio-temporal changes of volcanic pressure sources underground. Volcanoes inflate before eruptions because of magma ascent in the conduit and/or accumulation of magma in the chamber, and deflate during eruption because of withdrawal of accumulated magma/gas underground. These volcano inflation and deflation are measured by gedecitc sensors such as InSAR, GNSS, tilt meters and strain meters. Especially, tilt and strain meters can detect small changes of the ground deformation with high time resolutions which cannot be obtained by GNSS and InSAR observations.

Nishimura (2015a) examined temporal changes of pressure sources during eruptions at Ontake, Kuchinoerabu-jima and Shinmoe-dake in Japan by analyzing the JMA records athat are now available at active volcanoes. He showed that the tilt records are characterized exponential decay with time. And also, these changes are explained by magma pressure decrease due to Poiseulle flow or pseud gas flow, which are often used to describe the characteristics of eruptions. These are small phreatic or phreatomagmatic eruptions. Nishimura (2015b) further examined several vulcanian eruptions at Sakurajima volcano by analyzing JMA tilt records, and suggested that large eruptions seem not to follow exponential deays but indicate constantly decaying characteristics with time. Such constant decays are also observed at 2011 Shinmoe eruptions in which sub-Plinean eruptions are observed.

In the present study, we systematically examine the tilt records observed at Sakurajima volcano by using the JMA tilt records. We examine relations of tilt amplitudes caused by each eruptions with column height of eruptions. Also, acoustic signals and seismic signals associated with each vulcanian explosions are also compared with these observations. Preliminary results indicate that tilt recors are characterized by about three cases in which two steps of the changes are recognized during eruptions. We discuss the characteristics of tilt and column heights with radiationss of acoustic and seismic waves during eruptions to understand the mechanism, which is the basic information to evaluate the eruption magitudes.

Nishimura (2015a) Source process of small volcanic explosions as inferred from tilt records: Shinmoe-dake, Kuchierabu-jima, and Ontake-san. 2015 JpGU meeting, Chiba, Japan.

Nishimura (2015b) Discharge rate of volcanic eruptions as inferred from observed ground deformation and conduit flow models, SATREPS “Integrated study on Mitigation of multimodal disasters caused by ejection of volcanic products” Workshop, Yogyakarta.

Source characteristics of explosion earthquakes at Sakurajima volcano using spectral ratio method

Mohammad Hasib, Takeshi Nishimura, Hisashi Nakahara
Department of Geophysics, Graduate School of Science, Tohoku University

It's quite important to investigate physical parameters that control the magnitude to understand the magma process in conduit during vulcanian eruption. But, systematic analysis of explosions focusing on their magnitudes are few. In the present study, therefore, we analyze hundreds of explosion earthquakes recorded at Sakurajima volcano using spectral ratio method, that can retrieve the source spectral information without being disturbed by heterogeneous structure, to clarify the source spectra differences between large and small explosion earthquakes. Also, we examine the differences of source spectra between direct and coda waves, which are excited by initial explosion and continuous ash emissions, respectively.

We analyze explosion earthquakes recorded at three stations operated by Japan Meteorological Agency (JMA) for the two years from 2012 to 2013. The three stations are located at distances about 3 km away from the active crater, (Showa crater). We classify the explosion earthquakes into 4 classes (I, II, III, IV) according to RMS amplitude. Then, we calculate spectral amplitude ratios of classes II, III and IV to the smallest class I by shifting time windows every 10 s from the onset to coda waves, because vulcanian eruptions continue to effuse volcanic ashes for several to tens of minutes.

The spectral amplitude ratios obtained at three components at all stations are characterized by a flat amplitude at low frequency range (about 1 Hz- 2 Hz), a gradual decrease with frequency at an intermediate frequency range (about 2 Hz – 4 Hz), and a flat amplitude at high frequency range (about 4 Hz –10 Hz). Flat amplitude ratios at the low and high frequency ranges change according to the magnitude of classes, but no significant change is recognized in corner frequencies at about 2 Hz and 4 Hz. This observation may not be consistent with the scaling relation found for explosion earthquakes at several volcanoes, in which the source time duration and peak amplitude of force are controlled by vent radius under a constant pressure in the conduit (Nishimura and Hamaguchi, 1993). Since the explosion earthquakes at Sakurajima volcano occur at a same crater that does not change its vent radius significantly, the observed spectral amplitude ratio change can be attributed to pressure changes in the conduit.

We further examine source spectral ratios of explosion earthquakes for direct and coda waves. Although the corner frequencies are almost same, the flat amplitude ratios at the low and high frequency ranges decrease with lapse time. Such changes must reflect the difference of eruption styles during the vulcanian eruption: direct wave is associated with the initial explosion with strong air-shock and seismic waves, while coda wave is related to continuous ash emissions following the initial explosions. Since spectral amplitude ratios for different components at each station are almost same for direct and coda waves have same characteristic, the source mechanism of explosion earthquakes is almost same between the initial eruption and continuous ash emission. Hence, temporal changes in amplitude ratio strongly suggest that characteristic of source time functions exciting explosion earthquakes changes during vulcanian eruptions.

Acknowledgements: We used JMA seismic records.

Study on behavior of debris flows containing fine sediment from volcanic region

○K Nakatani (Kyoto U.), Y Satofuka (Ritsumeikan U.), K Miyamoto (U. Tsukuba),

There are many studies about sediment transportation such as debris flows in steep mountainous area but most of them focused on large sediment. However, sediment distribution is large from fine particles to large rocks and characteristic is different in each mountains. Recently, debris flow containing high concentration with fine particles occurred in volcanic regions, such as Izu Oshima sediment disaster occurred in 2013, and they have been reported to show high flow-ability comparing to stony debris flows.

However, the mechanism and behaviors of debris flows with fine sediment are not clear. From recent studies, it is presumed that some of the fine sediment behave as fluid phase instead of solid phase, but still remain as qualitative evaluation. To predict the run-off process, it is important to reveal the behavior and effect of fine particle in fluid phase and provide quantitative evaluation.

In this study, we conducted flume experiment as shown in Fig.1 with fine sediment (mean diameter 0.51, 0.29, 0.13 unit: mm) and coarse sediment (mean diameter 3.0 mm). We presumed that part of the fine particles contribute to increase the fluid phase density ρ when different size of particles exist. When the flow depth or deposition depth measured with the ultrasonic sensor was in a stationary state, we considered that sediment concentration is balanced to the slope. Fig.2 shows the relationship between slope degree and sediment (solid phase) concentration on experiment results and on Takahashi's equilibrium equation (1991, Takahashi). Smaller fine sediment cases show larger ρ such as 1.1-1.2 in 0.13 mm and around 1.1 in 0.29 mm. Next, we considered the ratio of fine sediment taken into fluid phase, and found that fine sediment concentration and flow condition of sediment mobility affect to the ρ increase. Therefore, we applied the ratio of friction speed to sedimentation velocity u_*/w_0 as parameter of fine sediment mobility condition. And compared with the ratio of fine sediment taken into fluid phase as shown in Fig.3. When u_*/w_0 becomes larger, the ratio of fine sediment taken into fluid phase become larger. One plot shows larger than 100% in 0.13mm fine sediment; it was assumed that all fine sediment and part of coarse sediment was taken into fluid phase.

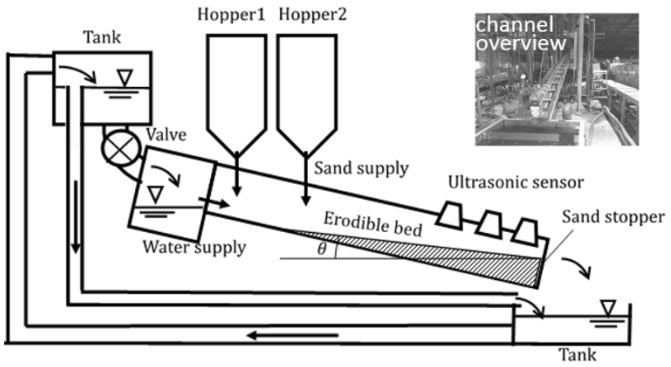

Fig. 1 Experimental flume outline.

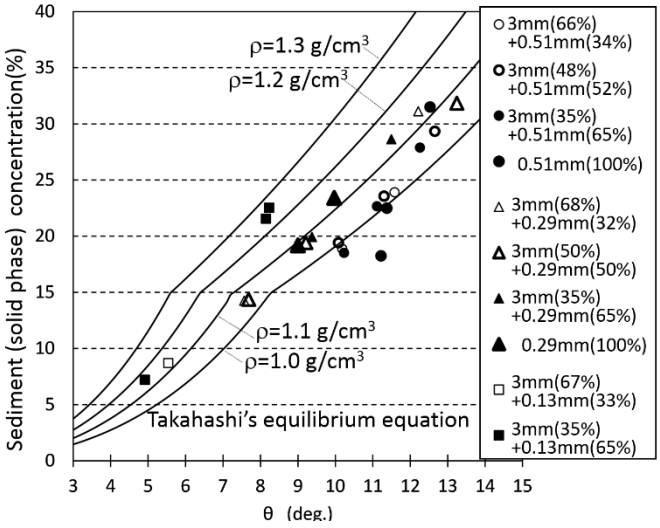

Fig. 2 Relationship between slope degree and sediment (solid phase) concentration on experiment results and on Takahashi's equilibrium equation.

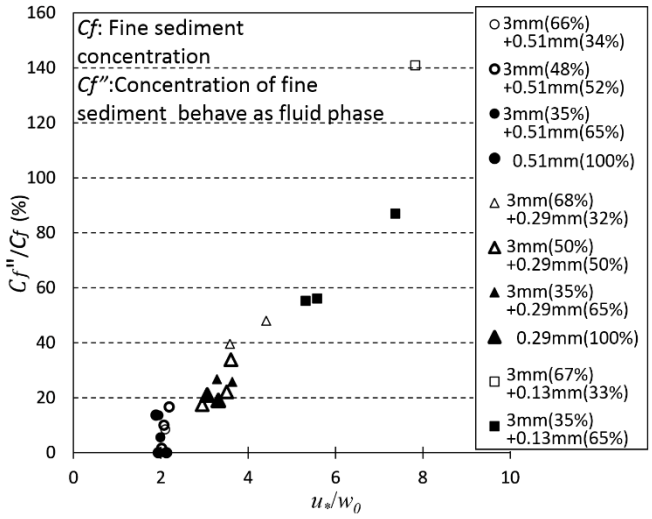

Fig. 3 Relationship between ratio of friction speed u_* to sedimentation velocity w_0 and ratio of fine sediment taken into fluid phase.

Sensitivity Analysis of Lahar Flow Simulation as Affected by DEM Resolutions

Adi Putri Anisa Widowati

(Research Assistant of Hydraulic Laboratory, Universitas Gadjah Mada)

Hydrology and hydraulic modeling that transforms rainfall into flow is essential for examining the response of a watershed on a certain intensity of rainfall. The watershed topography gives effect to the flow hydrograph characteristic. Recently, Geographic Information System (GIS)-based hydrology and hydraulic modelings have been widely carried out by researchers using Digital Elevation Model (MED) as topography data. Such modelings are important to be applied to examine the model's reability in simulating flood events over prone disaster areas such as Kali Putih watershed in Magelang, Central Java.

The modelling is carried out using both hydrology and hydraulic model. A GIS-based grid-based distributed hydrology model formerly developed by MIYATA is used to model the rainfall-runoff transformation. The topography data the model is SRTM data from USGS. The hydraulic model using 2 dimensional hydrodynamic flow SIMLAR is then carried out to simulate the flood processes in the stream and floodplain area. The important parameters such as infiltration coefficient and Manning's roughness number are obtained from literature and field observation images.

During the hydrodynamic flow modeling the data used is LiDAR DEM. The characteristics of the DEM which shows level of accuracy is spatial resolution. The different results of use of LiDAR DEM of 5 m, 10 m, and 20 m resolution in the modeling is then evaluated. The research is carried out firstly by applying modification of the initial LiDAR DEM data of 5 m resolution into topographic data of 10 m and 20 m resolution. using GIS application by bilinear interpolation method resampling technique. The sediment extents of simulation results are compared with the field sediment extent to examine the difference.

The simulation results show that the lower the DEM resolution produces the wider sediment extent of the simulation results. The simulation results also produces branches of sediment extent out of the actual lahar flow path in Kali Putih, while the branches of sediment extent do not exist during the field event. The area of the sediment extent branches increases as the DEM resolution decreases.

The Mineralogy of Lahars Deposits in Wlingi reservoir and its Role in Controlling Flushing Efficiency

○Dian Sisinggih (U. Brawijaya), Sri Wahyuni (U. Jember), Fahmi Hidayat (Jasa Tirta-1)

Sedimentation is the main problem in reservoirs and dams in Indonesia. Wlingi reservoir located in the middle of Brantas River, East Java, Indonesia is suffering from severe sedimentation due to heavily load of volcanic ash ejected from the eruption of Mt Kelut. The authority (Jasa Tirta-1) has been regularly conducted the coordinated sediment flushing at Wlingi Dam to release sediment. Flushing sediment in the reservoir Wlingi has been considered as an effective effort in removing the deposited sediment and it also can overcome the problems of degradation of the riverbed in the downstream of Brantas River. In any flushing events, not all the deposits can be flushed; particularly the cohesive and consolidated material was still remaining and it reduced the flushing efficiency. Especially for cohesive sediment, clay minerals have primary roles in controlling the size, shape, physical and chemical properties of the sediment particles. Characteristics of clay mineral of deposited sediments can be used to understand the properties and behavior of material movement and determine its interaction with the flows. The study aimed to obtain the characteristics of cohesive sediment deposition in the reservoir Wlingi and its implications in evaluating the effectiveness of sediment flushing. The grain size, magnetic susceptibility, X-ray diffraction (XRD), X-Ray Fluorescence (XRF) and Scanning Electron Microscopy (SEM) analyses has been conducted.

Results indicated that the grain size gradation of sediments in the upper, middle of the reservoir was dominated by sand material and the lower reaches were dominated by silt-clay. The volcanic ash from Mt. Kelut was identical with the majority of the deposited materials. It found that the mineralogical features of deposited sediment highly contained of elements of ferromagnetic (Fe, Al, Ni and Si), followed by the elements of diamagnetic (Si, Cu, and Zn), the element of paramagnetic (K, Al, Ca, Ti, and Mn), as well as elements anti ferromagnetic (Figure 1). The magnetic susceptibility of sediment had a high consistency ranges from 10.452 x 10^{-6} kg / m^3 and it indicated a group of natural mineral magnetite as known of the mineral Quartz (SiO_2), Fayalite (Fe_2SiO_4), Anorthite ($CaAl_2Si_2O_8$), Albite ($NaAlSi_3O_8$), Cristobalite (SiO_2), Enstatite ($MgSiO_3$) and Diopside ($CaMgSi_2O_6$). At the upstream part, there was the dominant mineral Kaolinite ($Al_2Si_2O_5$), Natrolite ($Na_2Al_2Si_3O_{10}2H_2O$), Nacrite ($Al_2Si_2O_5(OH)_4$), Pyrophyllite ($Al_2Si_4O_{10}(OH)_2$).

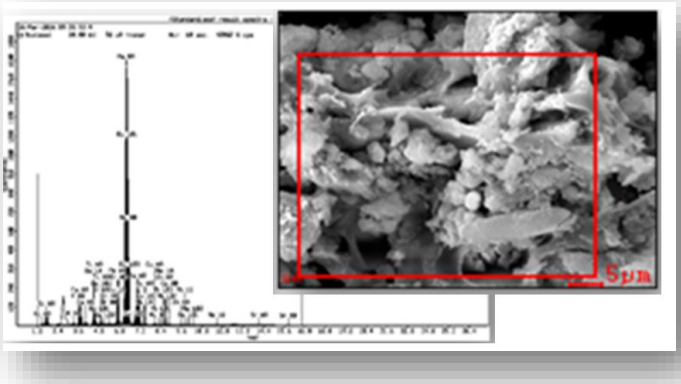

Fig. 1 The example of XRF and SEM results of Lahars deposits in Wlingi Reservoir.

The efficiency values are calculated based on the ratio storage capacity between after flushing (V_2) and before flushing (V_1) with original capacity of reservoirs (V_{ori}). The flushing efficiency was achieved ranges between 10-30% as shown in Figure 2. In order to increase the flushing efficiency in the next events and by considering with mineral properties that existed in cohesive sediment of Wlingi Reservoir, the specific examination needs to be carried out in the laboratory to get the appropriate flow parameters for the erosion/deposition of cohesive sediment. Another way is by mechanically removing the remaining cohesive sediment.

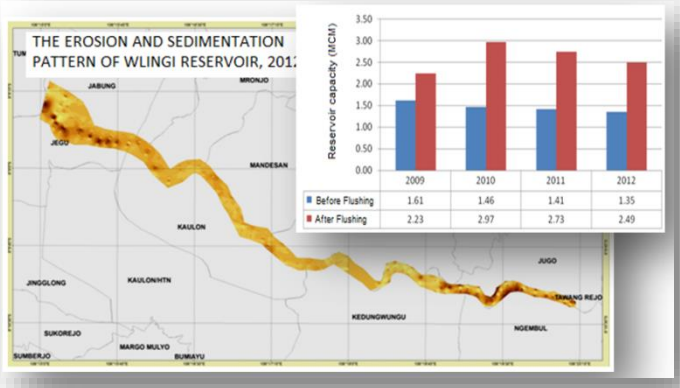

Fig. 2 The reservoir bathymetry and its life capacity before and after flushing, 2012.

An example of pyroclastic flow hazard mapping at Mt. Merapi by using numerical simulation

°K Miyamoto, M Shimomura (U. Tsukuba)

Numerical simulation is useful to understand and to evaluate the phenomena. Every quantity such as the velocity, the thickness of the flow, the deposition thickness of the pyroclastic material, and so on can be obtained at every time step, at any place. The result of the simulation depends on the conditions such as the topography, the scale of the pyroclastic flow, the derection of the decending, and so on. We need to give such conditions to the simulation, and we can get the results corresponding to the conditions. It means that we can estimate or evaluate any possible, potential pyroclastic flow disaster by giving the suitable conditions.

The other hand, to predict current conditions such as potential scale of the pyroclastic flow, decending direction, and so on, we need to observe volcanic activity. If we will be able to predict such conditions from the monitoring, we can do the real time simulation, by putting them into the simulation.

Today, computer power become quite high, however it is still not enough to conduct real time simulation. Therefore, it is necessary to prepare a set of possible, potential pyroclastic flow simulation results. When we will identify the current conditions by the monitoring, we will be able to search the suitable resurts from the set of simulation results, which would be simmilar with real time simulation results. By using such suitable simulation results, we could prepare suitable hazard map, and the map could be rearranged correspond to the changing of the conditions.

Fig.1 shows an example of such hazard mapping method. There are two components, which are a set of numerical simulation and the predicting method of the conditions, which are used in the simulations. Based on the monitoring, we can draw a hazard map at any, every necessary time by selecting suitable cases of simulation result from the set of simulation results and by compiling the selected results.

Fig.2 is an example of a set of hazard maps, which are prepared based on the concept mentioned above. We conducted totally 40 cases of the simulations, which are 10 decending derections and 4 magnitude/volumes of pyroclastic flows, which are 1.0, 3.0, 10 and 30 million cubic meter. The topography, DEM data used for the simulation is 10m resolution rearranged from ALOS-AW3D (©RESTEC, NTT DATA/Included ©JAXA).

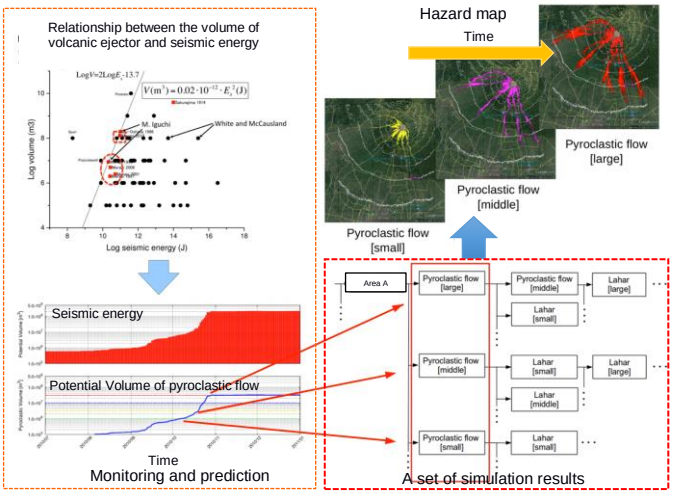

Fig.1 Schematic figure of a hazard mapping method using numerical simulation

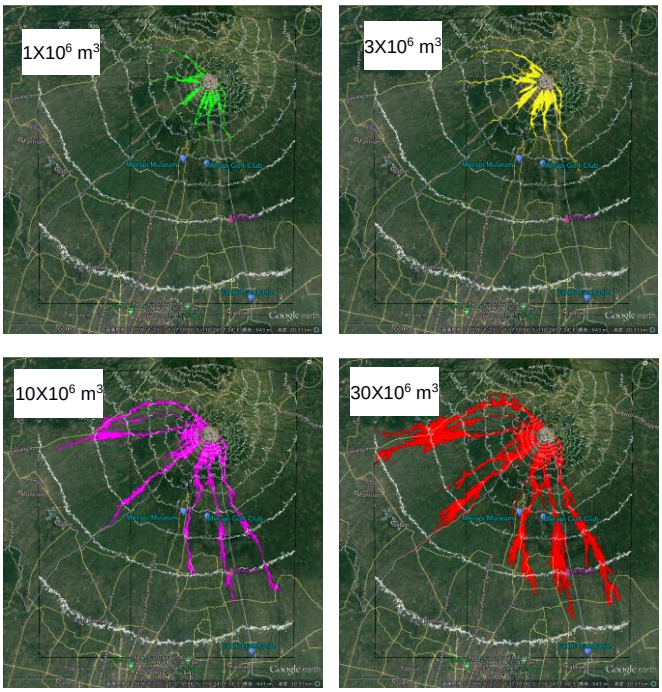

Fig.2 An example of a set of hazard maps

Cloud Based Observation System

°Dicky Hadiyuwono, Djoko Legono (UGM), Dwi Kristanto (Balai Sabo)

An easy to user and high availability access of observation data is an important tool in assisting researchers' dan public to calculate and evaluate potential hazard around Mt. Merapi. After careful evaluation of potential benefits and drawbacks of cloud based system in comparison with standard server configuration, we proceeded in developing a cloud based system taking caution of its drawbacks and implementing the necessary measure to limit its effects.

The system consists of real-time data communication system to remote sensor, scalable cloud server architecture. A web based interface was chosen mainly due its ease of use and familiarity but is also more secure rather than letting user access the server directly. Social based authentication was also used to increase accountability and prevent login sharing among users. Using the provided interface has increased productivity among researchers focusing primarily analyzing rather than processing and visualizing the raw data. In the server infrastructure redundancy and failover has been implemented in every layer to ensure the security and high availability of data.

By integrating simulation system that have been developed by other researcher and more data from BPPTKG and Balai Sabo, an active analytics and forecasting system can be developed in the near future. Providing up-to-date hazard maps and alerts of potential hazard.

The cloud based system has proven not only easy to use and scalable but also reduce the operating cost drastically.

Progress of development of simulation and observation integrated database system

○M Shimomura, K Miyamoto (U. Tsukuba), M Iguchi (Kyoto U.),
IGM Agung Nandaka, Agus Budi Santoso, Sulistiyani, Prayitno (BPPTKG)

A disaster is recognized as many types and scales of events. And a result of event sequentially affects to following event. Such complex and multiple event chains, that is "multimodal", lead less understanding of the disaster itself. To understanding a multimodal disaster, overall of potential chains should be investigated. Because a large number of variations and uncertain factors of the chains should be considered. According to this concept, an actual disaster would trace on a path of the chains.

A numerical simulation is suitable for analyzing the potential chains. An observation is necessary to evaluate the event and to extract the path from the chains. Therefore, both simulation and observation results should be integrated in a database. To efficiently utilized the database, interface/application program interface (IF/API) should be developed.

Such under developing integrated system has been installed at BPPTKG. The structure of the system is shown in Fig. 1. The data from observation and simulation systems are collected in the database throughout a gateway. The gateway is consisted by IF/API for database, simulation and observation systems, scenario editor etc. The simulated result should be stored according to the structure of event chains. The observation data should be stored according to contents and date. The database is developed as hybrid physical and logical database to improve scalability and portability e.g. easy browsing and quick extracting the event chain. A schematic diagram of data flow at BPPTKG is shown in Fig. 2. In Fig. 2, yellow box shows the gateway and brown one shows the database. The volcanic and hydrological observation data are corrected in the database via the gateway. The simulation system can access the database via the gateway.

A pyroclastic flow is one of the most disastrous event of volcanic disasters. And the pyroclastic flow can be recognized as 1st event at the chains. By using the system, the extraction method of the pyroclastic flow has been developed (Fig. 3).

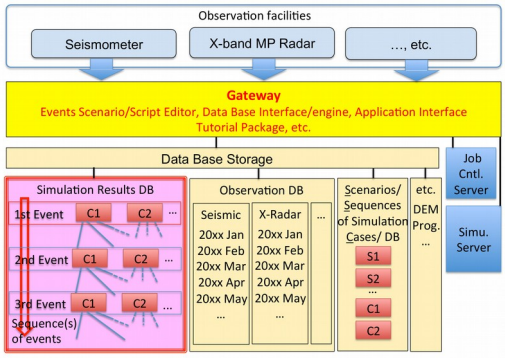

Fig. 1 Structure of integrated system at BPPTKG.

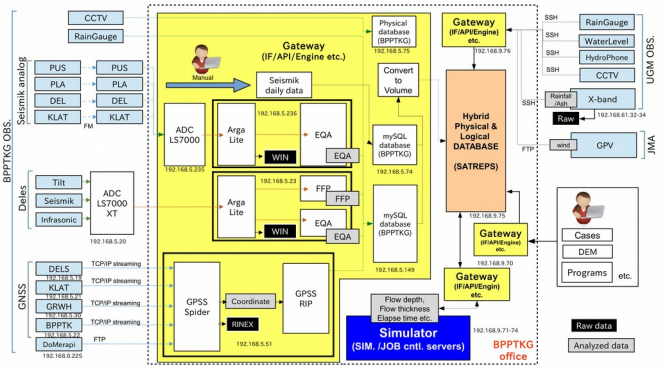

Fig. 2 A schematic diagram of data flow at BPPTKG.

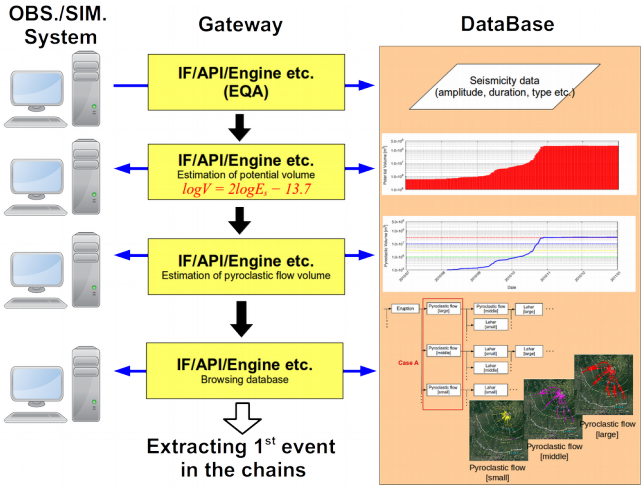

Fig. 3 Example of extracting the event chain from the database in case of pyroclastic flow.

Utilization of X-band radar information for lahar Early Warning System (EWS) at Mount Merapi

Arif R. Mulyana, Samuel J. Sutanto, Akhyar M. *)

*)*Sabo Technical Center/Balai Litbang Sabo, Research Center for Water Resources, Ministry of Public Works and Housing, Indonesia*
Jl. Sabo 1, Maguwoharjo Depok Sleman, Yogyakarta 55282, Phone: +62-274-886350

Abstract

The sediment related disasters such as landslide and debris flow are categorized amongst the biggest disasters in Indonesia. Based on the number of casualties, the disaster caused by volcano eruption is placed as the second deadly disaster after earthquake and tsunami (dibi.bnpb.go.id, 2015). The materials, which come from the eruption, can cause the debris flow disaster known as lahar. The threat of the lahar disaster in Indonesia is considerably high because Indonesia has 129 active volcanoes. Balai Litbang Sabo, therefore, is developing an Early Warning System (EWS) for lahar disaster, which can give a warning signal several days before the disaster occurred. This system is constructed based on daily precipitation forecast results obtained from Indonesian Agency for Meteorology, Climatology and Geophysics (BMKG) and an EWS platform named Delft-FEWS. The lahar model results (SIMLAR) with various precipitation inputs will also be stored in this platform. Furthermore, this platform will process both near real time precipitation data (TRMM satellite) and forecast data (BMKG-ECMWF). Based on the forecast data, the warning will be given and the SIMLAR result with the forecast precipitation will be displayed in the Delft-FEWS platform when there will be high precipitation potency for one, two, and three days ahead (Figure 1).

Though the under developed EWS system is adequate to produce lahar warning system, the uncertainty in the precipitation forecast data using BMKG-ECMWF climate model remains high. On the other hand, the utilization of weather radar owned by Balai Litbang Sabo shows a promising tool for lahar EWS. The cross correlations between radar and in situ observation data are quite high, with correlation values (R) of 0.68-0.82 (Figure 2 left). The precipitation lag time of 30-60 minutes produced by the radar indicates a promising opportunity for lahar EWS (Figure 2 right). A combination between BMKG forecast data for daily warning system and X-band radar data for hourly warning system will be a robust system, which can give a more reliable and accurate warning. The utilization of X-band radar for lahar EWS will be incorporated in the Delt-FEWS platform under the Balai Litbang Sabo research budget year 2017.

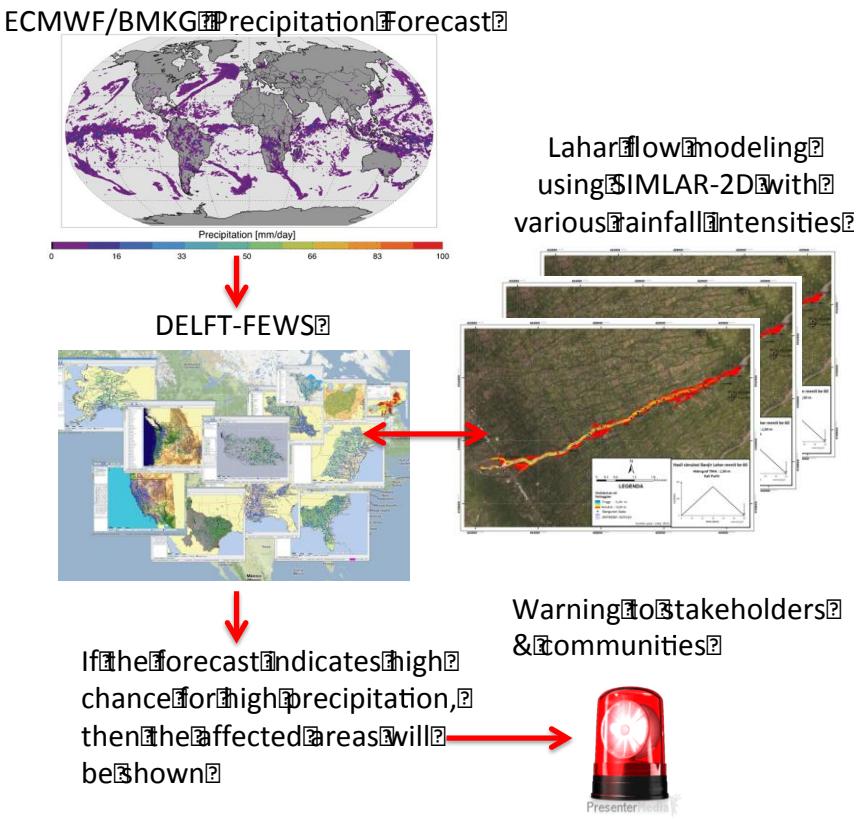

Figure 1. Delft-FEWS system for lahar early warning.

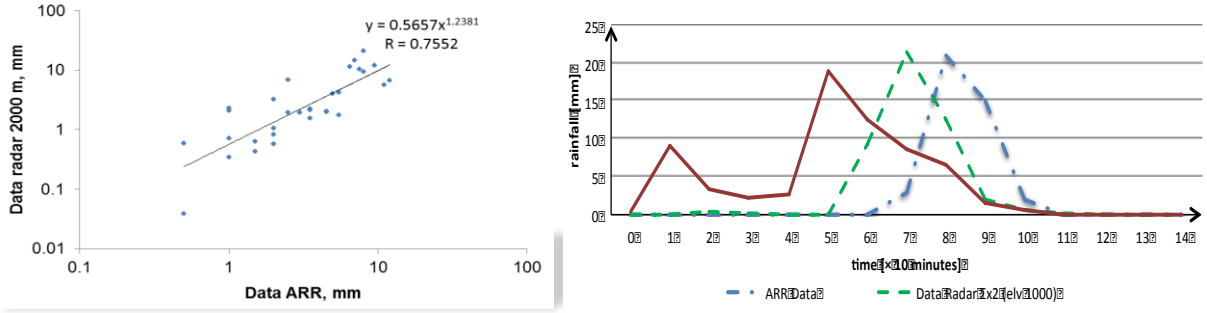

Figure 2. Precipitation correlation obtained from radar and in situ observation (left); Lag time between radar data and in situ observation data (right).

Installation of Volcanic Ash Dispersion PUFF Model to BMKG Indonesia

Kurniaji (BMKG), Hiroshi L. Tanaka (U. Tsukuba)

Indonesia has 127 active volcanoes which is in the last 3 years 5 of them often erupt. These four volcanoes are Sinabung, Dukono, Raung, Tengger Caldera/Bromo and Rinjani. Volcano eruption resulted in many losses and damage to both humans and the environment associated with different types of materials that they produce. Lava and volcanic ash released by the volcano could make hazards for public civilization, and transportation especially for Aviation. BMKG (as NMHS), CVGHM (Ministry of Energy and Mineral Resources) and DGCA (Ministry of Transportation) have responsibility to manage and handle the hazards caused by Volcano Activity (VA) especially for aviation safety.

Related to this responsibility, BMKG always issue the graphic of RGB Image of Himawari-8 weather satellite three hourly every day to give concise information related the coverage and movement of VA. Unfortunately satellite imagery cannot detect VA due to embedded cloud, especially in tropical area where atmosphere is more humid by a lot of water vapor. Direct visual information delivered by CVGHM from volcano site also still not very helpful to cover this deficiency (Fig. 1.1 – 1.3). This condition force BMKG to rely on VA forecast from BOM (VAAC-Darwin), although sometimes trapezoidal coverage of VA forecast from VAAC-Darwin often too large compared to the actual conditions.

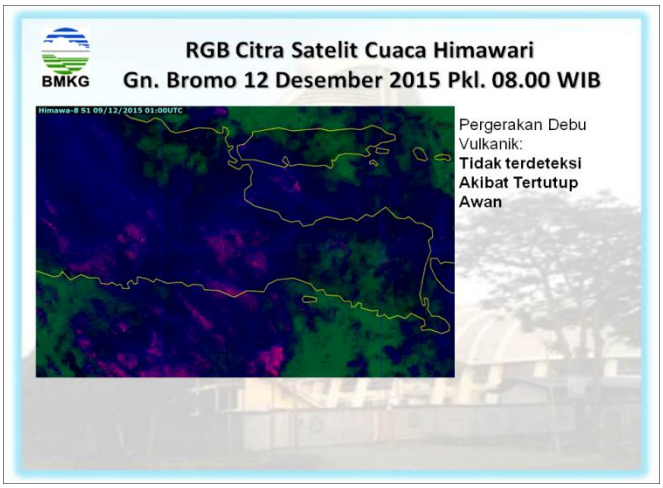

Fig. 1.1 RGB Analysis of Himawari-8 Weather Satellite Product (Bromo, December 12th 2015 01 UTC)

Fig. 1.2 CVGHM/on site Ground Observation (Bromo, December 11th 2015)

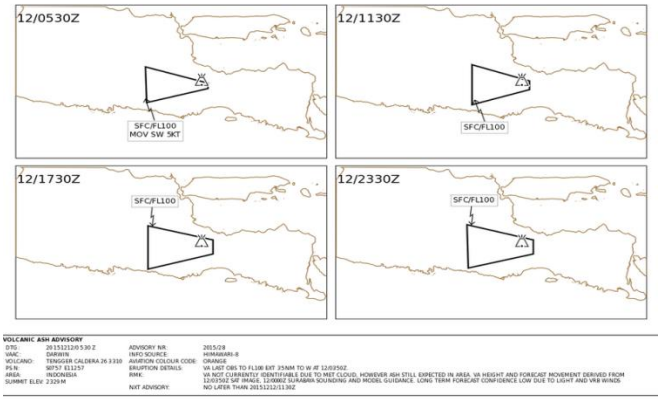

Fig. 1.3 VAAC-Darwin Volcanic Ash Advisory (VAA) (Bromo, December 12th 2015 05.30 – 23.30 UTC)

Related to this current issue, through JICA-SATREP program, BMKG had send two operational personnel to be trained well by expert in Tsukuba University in order to learn how to forecast VA spread in the atmosphere using PUFF Model which has been develop by Prof. Hiroshi Tanaka of Centre for Computational Science (CCS) of Tsukuba University (Fig.2). The one month training guided by Prof. Tanaka ran quite well and our personnel have understood how to run PUFF model before the end of training.

Fig. 2 Training Activity with Prof. Tanaka, Prof. Iguchi and Student of Prof. Tanaka

BMKG begin to build environment which is as similar as Prof. Tanaka has at CCS and now staff of BMKG Centre of Aviation Meteorology is able to operate the PUFF Model, but its accuracy still need to be improved (model adjustment based on the eruption characteristics of target volcanoes; information on estimation of eruption rate from CVGHM as additional parameter for model input). Figure 3 below show the result of PUFF model running due to eruption of Rinjani Volcano September 27th 2016 which is quite big eruption during the last 3 months.

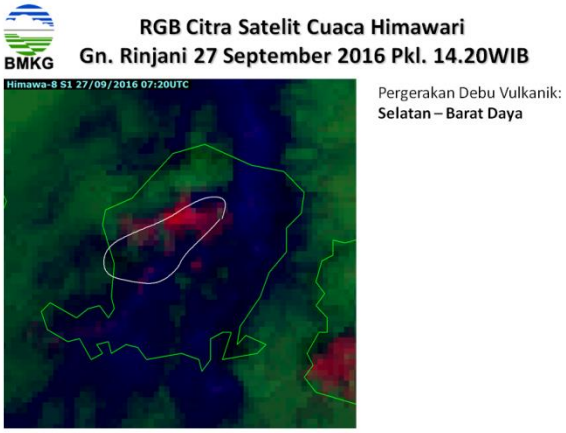

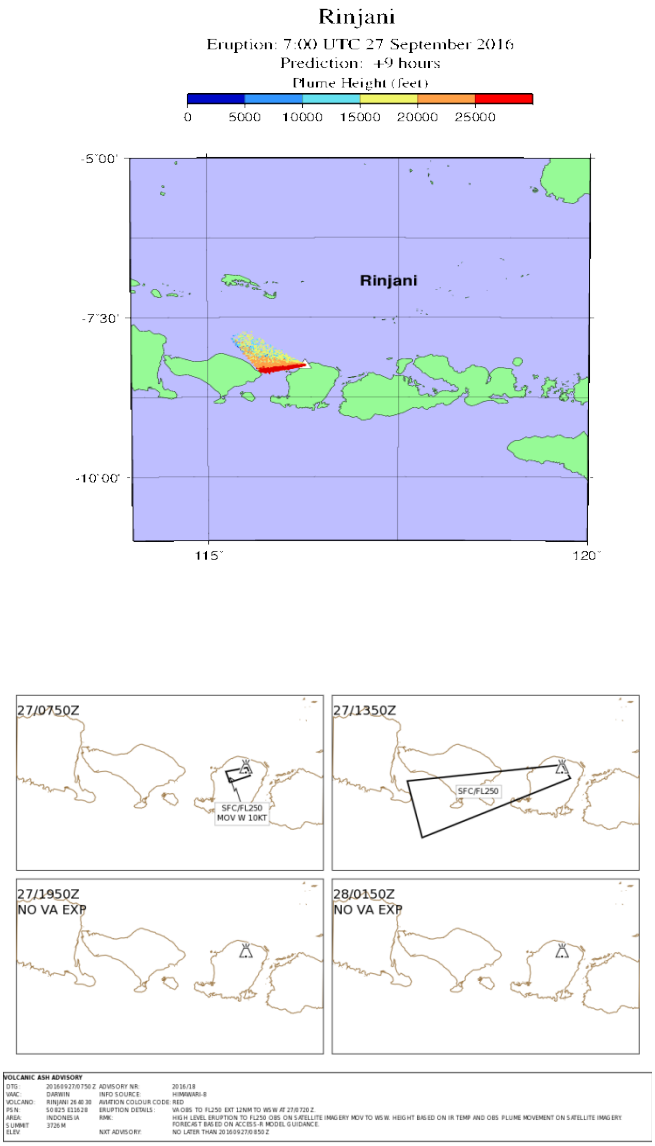

Fig. 3 RGB Analysis of Himawari-8 (top), Ash Plume Dispersal from PUFF model (middle), and VAA from VAAC-Darwin (bottom) (Case: Rinjani Eruption Sept 27th 2016)

The plume dispersal image from PUFF model show similar direction for the movement of VA up to 9 hours after the eruption compared with forecast from VAAC-Darwin if we insert same plume height (tt) value which is used by VAAC-Darwin (FL250). It describe not only VA movement on 25.000 feet but also VA movement from 5000 until 20.000 feet although the forecast accuracy have to be questioned because the absence of real data emission from CVGHM. While waiting for the coordination with CVGHM due to this data, BMKG Centre of Aviation Meteorology has been running the PUFF model daily and restoring the output in aviation system. The launching of the PUFF model output on BMKG aviation website also being postponed related to this issue.

Determination of the mass eruption rate for the 2014 Mount Kelud eruption using three-dimensional numerical simulations

○Y. J. Suzuki (U. Tokyo) and M. Iguchi (Kyoto U.)

In order to reconstruct or predict the progression of volcanic eruptions, estimations of eruption conditions at the vent from observable quantities such as plume heights have long been a major focus of research in volcanology. In this study, we present 3D numerical simulations for the 2014 Kelud eruption. We aim to comprehensively explain the data obtained by various observations and to constrain the eruption conditions at the vent and, in particular, the mass eruption rate (MER).

The 3D numerical simulations were designed to emulate the injection of a mixture of pyroclasts and volcanic gas from a circular vent located at 1500 m above sea level (asl.). We used a combination of a pseudo-gas model for fluid motion and a Lagrangian model for particle motion. Atmospheric conditions were based on the meteorological reanalysis data provided by the Japan Meteorological Agency's Non-Hydrostatic Model at 16:00 UT on 13 February 2014. We carried out seven simulations of eruption plumes with variable MER ranging from 5.0×10^5 to 7.0×10^7 kg s^{-1}. The other parameters were kept fixed in all of the simulations. Magmatic temperature and water content were assumed to be 1273 K and 5.0 wt.%, respectively.

The parametric study indicates that the field observations can be explained when the MER of this eruption was 3×10^7 to 4×10^7 kg s^{-1}. For these MERs, the eruption column reached 23–32 km asl. and the umbrella cloud spread at around 18 km asl. (Figs. 1 and 2). A parcel of eruption clouds drifted downwind from the overshooting top, which was also observed by CALIOP LIDAR. The horizontal expansion of the umbrella cloud simulated by the present model was also roughly consistent with the satellite images (Fig. 3). The area of simulated umbrella clouds was proportional to $t^{4/3}$, which agrees with a simple model of axisymmetrical gravity current. This means that although the simulated umbrella cloud develops asymmetrically, its lateral evolution can be approximately described by the simple gravity current model.

Our estimation of MER corresponds to the minimum value of the estimation from field observations ($6.5 \pm 2.8 \times 10^7$ kg s^{-1}; Maeno et al., submitted). One possible explanations for the small difference between these two estimations is the uncertainty of the field observations. Another possible explanation may be attributed to the pseudo-gas assumption in our model. In the pseudo-gas model, all the pyroclasts ejected from the vent are assumed to enter the umbrella cloud. With the pseudo-gas assumption, the mass and volume of the umbrella cloud will be underestimated or overestimated in the simulations.

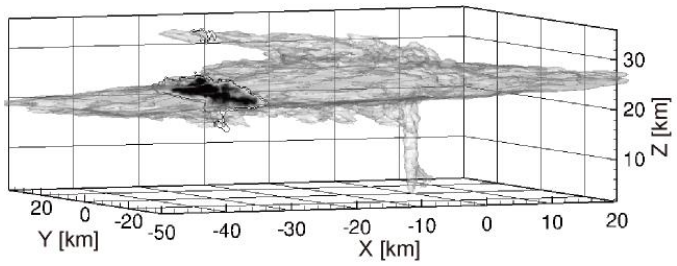

Fig. 1 3D simulation result of the 2014 Kelud eruption. Iso-surface where the mass fraction is 0.02 at t = 1800 s and the vertical cross-section at x = –30 km.

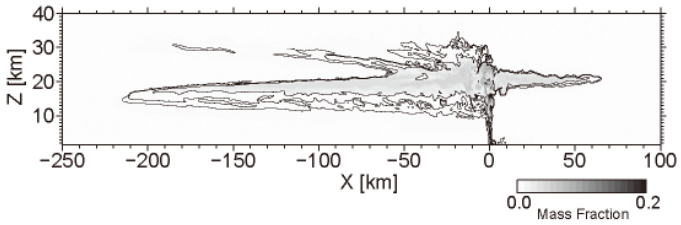

Fig. 2 The vertical cross-section of the mass fraction of the erupted material at y = 0 km and t = 7200 s.

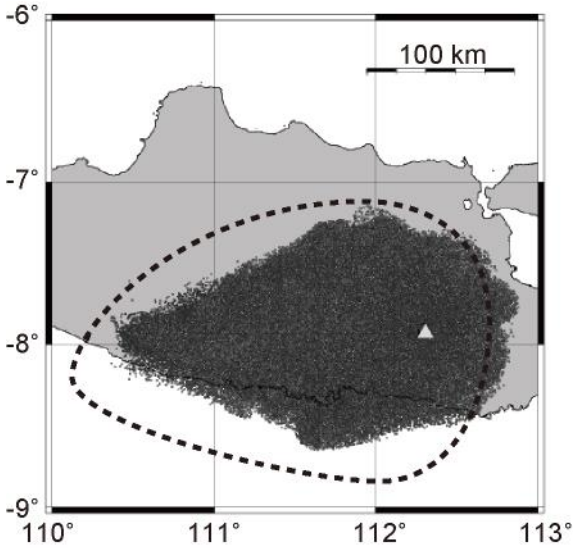

Fig. 3 Simulation results of umbrella cloud expansion. Dashed curve represents the edge of the observed cloud.

Comparison of Volcanic Ash Dipersion Using PUFF Model with RGB image from Himawari-8 Data

Andersen Panjaitan (BMKG)

Mount Raung has frequently erupted from mid to end July 2015. On 16 July 2015, due to dispersion of volcanic ash from Mount Raung, Transportation Ministry announced that all flight from Juanda International Airport would be grounded from 1.20-7.20 pm local time. It caused almost than 900 flights were canceled or delayed when thousands passenger had planned return to Surabaya to celebrate the end of Ramadhan. An accurate forecast model for volcanic ash distribution is needed to give suggestion when airport can be opened.

PUFF is a trajectory model developed for tracking ash clouds for hazard mitigation, especially to aircraft. The model can be used as a forecast tool to predict cloud migration and dispersion, an operational tool that provides near real-time volcanic cloud positions. Lagrangian random walk formulations to calculate a trajectory for a user-specified number of particles is used by the model, and it also calculates turbulent diffusion and particle fallout.(Searcy et. al, 1998)

Himawari-8 is a new geostationary satellite which starting being operational on July 2015, just few weeks before Raung eruptions. With 16 channels and 10 minutes temporal resolution, it brings an advantage to get higher frequency in monitoring cloud include volcanic ash. Prata and Grant, 2001, consider strong correlation between the difference in brightness temperatures in the split window channels and precipitable water is an indicator of volcanic ash detection by satellite. Japan Meteorological Agency (JMA) shows combining split window channels by RGB method is easy and fast technique to distinguish between volcanic ash and other geographical objects. Some modification in the RGB recipe has made to enhance the color contrast, where the recipe become 10.4µm-12.4µm, 3.9µm-10.4µm, and 3.9µm for red, green, and blue component, respectively.

The dispersion volcanic ash from PUFF model (Fig. 1) is evaluated with RGB image from the satellite (Fig. 2). With the proper height eruption estimation, it show PUFF model with Global Spectral Model (GSM) initial data can well described the migration of volcanic ash. At 9 hours prediction after Juanda Airport closed (22 UTC), PUFF model predicts volcanic ash eruption will be transported westerly. The prediction is similar with observation by satellite, thus the performance of the model is subjectively good. However, in term of operational purpose, some parameters for input model are not available by observations and potentially bring significant error in prediction.

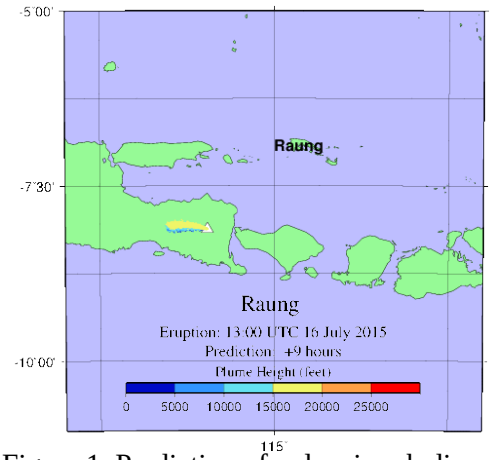

Figure 1. Prediction of volcanic ash dispersion using PUFF at 22UTC

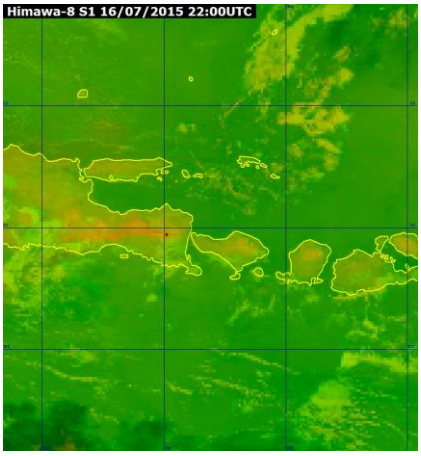

Figure 2. Volcanic ash from Mount Raung is indicated as red plume

Three-dimensional view of volcanic ash clouds based on weather radar data

○M. Maki (Kagoshima U.), I. Suzuki, S. Takahashi, M. Iguchi (Kyoto U.)

The present paper outlines three-dimensional visualization of weather radar data of volcanic eruption columns and ash clouds from Sakurajima volcano in Kagoshima, Japan.

The methods commonly used to monitor volcanic eruptions and ash clouds are based on passive measurements such as visual observations, automated monitoring with highly sensitive cameras, and observations by geostationary meteorological satellites. Such methods or instruments are effective during daytime hours and under fine weather conditions. However, they become significantly less useful when an eruption occurs under cloudy or rainy conditions. It is also difficult for passive sensors to measure the internal structures of eruption columns and ash clouds. To solve these problems, the present study focuses on the usage of weather radar to observe volcanic eruptions, which has been utilized since the late 1990. We analyzed data of Sakurajima volcanic eruptions which were observed by operational X-band polarimetric radar. The radar is set up in Tarumizu in 2011 and operated by the MLIT (Fig. 1). Figure 2 shows the antenna scan strategy adopted by the MLIT: volume scan data with antenna elevation angles from 1.7° to 20.0° are obtained at 5-minute intervals.

Three-dimensional analysis tools of weather radar data were developed by Kagoshima University to investigate the internal structures of volcanic ash columns and clouds. The analysis tools can obtain three-dimensional distributions of polarimetric radar parameters that can be used to examine the inner structures of ash columns and ash clouds and to retrieve the ash cloud echo top height, the ash cloud volume and amounts, and the ascent or descent speeds of pyroclastic materials, etc. The analysis tools were applied to the volcanic eruption occurred on 18 August 2013.

Figure 3 is a schematic picture which explains interpolation procedures of Plan Position Indicator (PPI) data at an arbitrary time and elevation angle. A set of interpolated PPI data are used to construct Constant Altitude PPI (CAPPI) data. The interpolation algorithm is based on advection vector calculated by a correlation method of two consecutive PPI reflectivity images. A

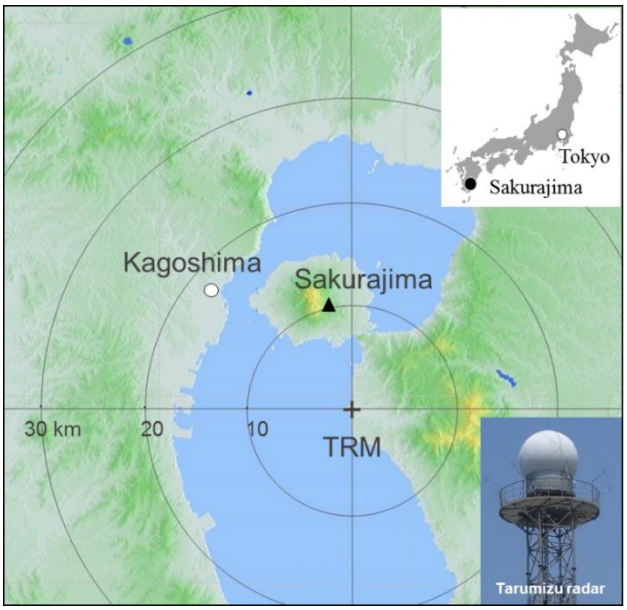

Fig. 1 Map showing locations of Sakurajima volcano and X-band polarimetric weather radar operated by the Ministry of Land, Infrastructure, Transport and Tourism (MLIT) Japan. The radar is set up in Tarumizu (TRM) which is located 10.7km from the Showa crater of Sakurajima volcano.

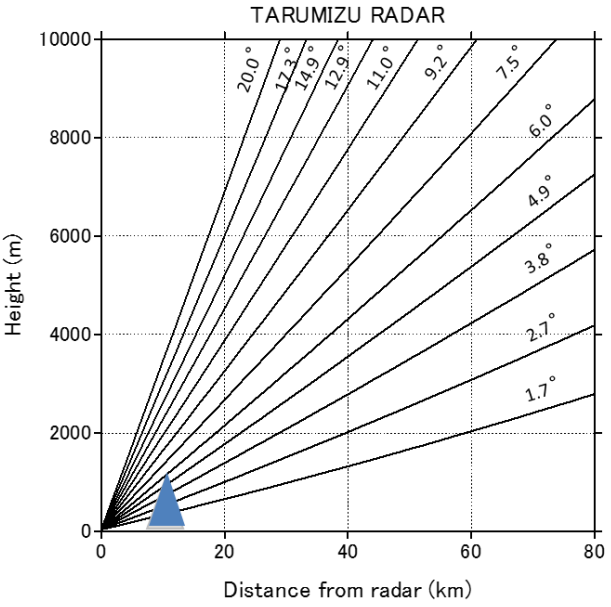

Fig. 2 X-band polarimetric radar antenna scan strategy. Numbers in the figure shows elevation angles. A triangle shows the location of Sakurajima volcano.

morphing technique is also used in the interpolation.

Figure 4 shows an example of 3-D view of analyzed radar data of Sakurajima volcano eruption column observed at 07:41:30 UTC, Aug. 18, 2013. The inner structure is shown by a volume rendering technique. Vertical and horizontal cross section analyses may give us more quantitative information on eruption ash columns such as volume, reflectivity distribution, and pyroclastic vertical motion. Figure 5 shows the horizontal distribution and vertical cross sections of accumulated reflectivity of ash column from 16:32 to 17:30 LST of the Sakurajima volcanic eruption on August 18, 2013. The maximum accumulated reflectivity, i.e., the dense concentration of ash amounts, was located at about 3km west-northwest from the crater and at the height of about 800m above the crater. It is interesting the second maximum of the accumulated reflectivity is located at the height of about 3200m above the crater. This characteristic distribution of reflectivity on vertical cross section will be due to the size sorting phenomena of ash particles. The time series of 3-D images of reflectivity distributions effectively show the size sorting phenomena.

The preliminary results of the radar data analyses lead us to the conclusion that three-dimensional analyses of X-band polarimetric radar data help us not only intuitively but also quantitatively to understand the inner structure of the eruption column and its temporal change.

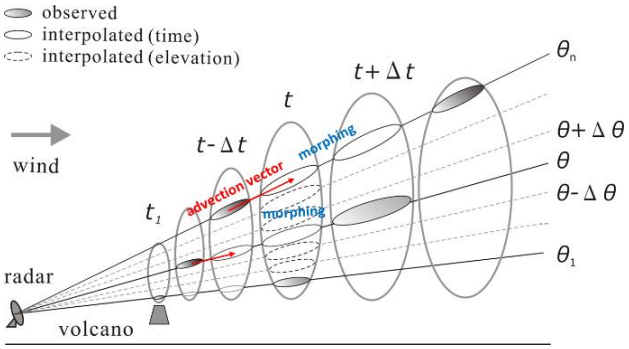

Fig. 3 Schematic picture of the time and temporal interpolation of volume scanning radar data.

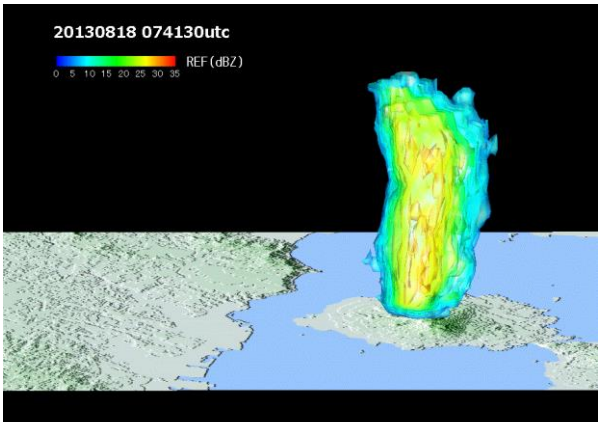

Fig. 4 Example of 3-D radar data view of the Sakurajima volcanic eruption on Aug. 18, 2013.

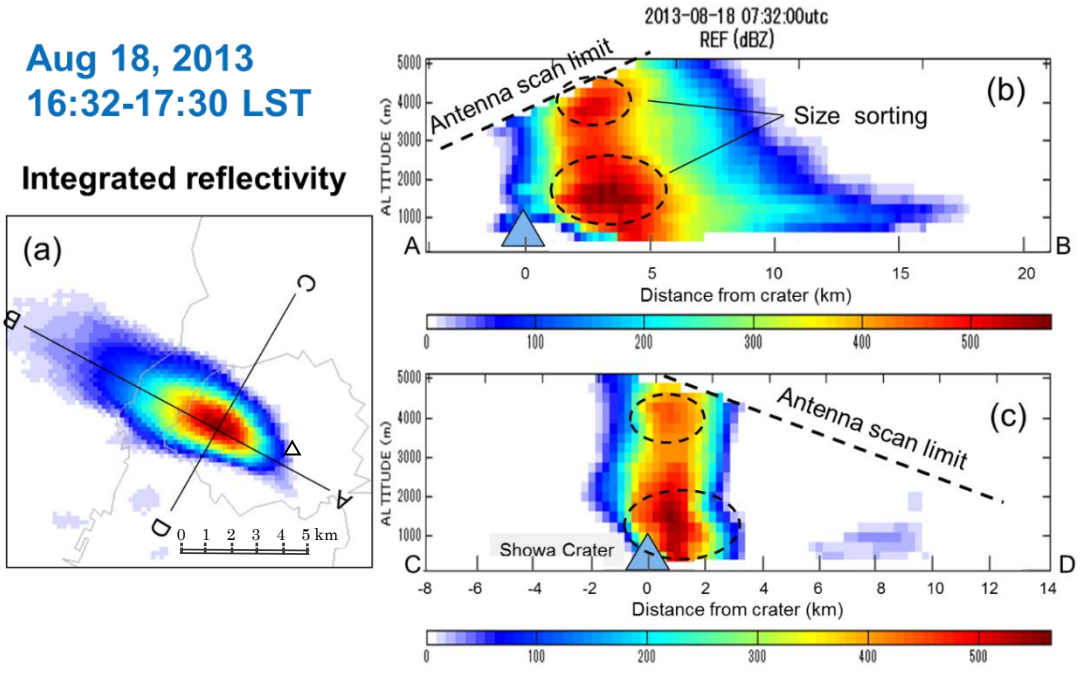

Fig. 5 (a) Horizontal distribution of accumulated reflectivity ash clouds, (b) vertical distribution along the line A-B, (c) along the line C-D. accumulation time is 16:32-17:30 LST, Aug. 18, 2013.

Development of Estimating Method for Volcanic Tephra Volume by Meteorological Radar

○Satoru Oishi (Research Center for Urban Safety and Security, Kobe University),
Masahide Muranishi (Graduate School of Engineering, Kobe Unuversity)

Volcanic eruptions often remain huge amount of unstable volcanic tephra consisting of volcanic ash, volcanic lapilli and volcanic bombs on the hillside of volcanoes. Sediment related hazards caused by these unstable sediment and severe rainfall are one of the most devastated disasters against human society. It is necessary to mitigate sediment related disasters by appropriate countermeasure which requires the amount of sediment remaining. Now, meteorological radar is expected to detect sediment remaining because it can estimate the accurate volume of volcanic tephra without field survey.

Amount of volcanic tephra by meteorological radar have been estimated from radar reflectivity factor (Z) and volcanic tephra drop size distribution (DSD). Radar reflectivity factor depends on DSD (N(D));

$$Z \propto \int_0^\infty D^6 N(D)\,dD = \int_0^\infty D^6 N_0 \exp(-\Lambda D)\,dD$$

where D is particle diameter in mm and N_0 and Λ are parameters determined by the DSD.

Fig. 1 shows diagram of estimating method for volcanic tephra by meteorology radar. In this method, we use X-band multi parameter radar, SRHI (Sector Range Height Indicator) scan. This scan mode detects vertical section in the sky and can capture eruption column above the crater. On the other hand, the ground truth data is obtained from Video Drop Size Detector (VDSD), developed for particle information (Suzuki, 2012), established around the volcano. The ground truth data includes DSD and median value of DSD (D_{50}). Using the radar and ground truth data, we can calculate the each high DSD;

$$N(D)_{h_{imm}} = N_{imm} \exp(-\Lambda_{imm} D)$$

where imm is median value of DSD in each hight. Fig. 2 shows time series of volcanic tephra after the eruption. All particles above the crater fall with flued by the horizontal wind. Based on this principle, we can calculate the DSD and volcanic tephra volume aligned on a straight line from the crater to the observation point on the ground.

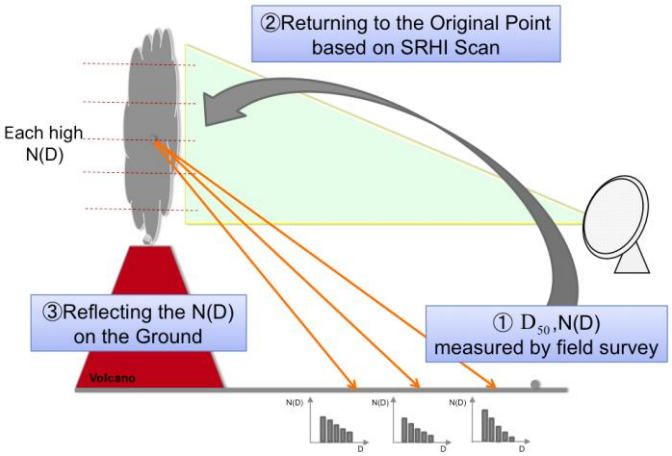

Fig. 1 Schematic chart of estimating the drop size distribution after the eruption based on SRHI scan by meteorological radar.

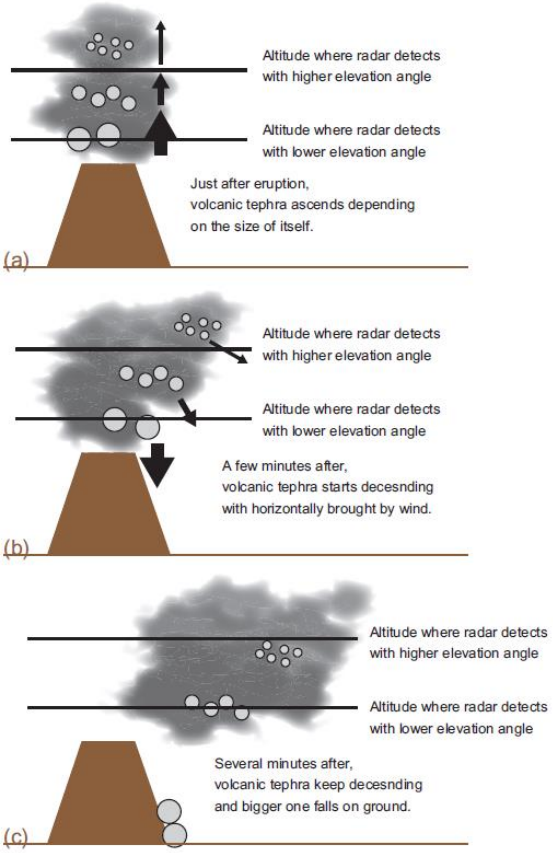

Fig. 2 Schematic image of time series change of volcanic tephra detected by radar.

Satreps, from Yogyakarta to National: seed for National-wide implementation

Dwi Kristianto, Arif R. Mulyana, Samuel J. Sutanto. [*)]

[*)]*Sabo Technical Center/Balai Litbang Sabo, Research Center for Water Resources, Ministry of Public Works and Housing, Indonesia*
Jl. Sabo 1, Maguwoharjo Depok Sleman, Yogyakarta 55282, Phone: +62-274-886350

Indonesia is subject to many different natural hazards or disaster due to its location in the Tropics, which is impacted by 129 active volcanoes, four earthquake belts, and rainy monsoon that cause annual flood, landslide, drought, lahar, and tsunami. One of the disastrous natural hazards is sediment disaster, including debris flow, lahar, landslide, and slope failure. These disasters are mostly triggered by mechanism process of water, soil, and often together with human activities. In Indonesia, the sediment related issues might deal with management for mitigation of sediment disaster, called SABO.

To anticipate the sediment related disaster problems, there are several actions that we can do such as increasing the action plan at vulnerability hazard areas, implementing the early warning system, increasing the control and supervision of the land use according to the regional space plan, increasing the recovery of damage, natural resources, and environmental conservation. Since Balai Sabo is a responsible agency for lahar early warning system in Indonesia, Balai Sabo has already established several tools for lahar early warning system in Mount Merapi areas such as telemetry system (rainfall and water level), CCTV, precipitation X-band radar, and vibration sensors.

Decision Support systems for sediment disaster management is complex in all aspect since the management needs continual, integrated, and comprehensive program applied by the government, people, and stakeholders. The government has applied the best disaster management practices and mitigation, however the lost/damage is still exists due to limited budget and complexity of the problems. Integration means a linkage in all aspect as well as dimensions and comprehensive implementation for broad coverage. The management substances are: human resources, natural resources, infrastructure, institution, financial, policy, legalization, and management capability. All of the management substances must be applied for raising the awareness of all stakeholders and societies to reduce the disaster impact. The guideline must be open and applicable for central, regional, and local government due to the different characteristics, situation, and condition of the areas.

Satrep project in several volcanoes especially in Merapi is a good example for best practice on disaster management and mitigation. Furthermore, Support System for Decision Making (SSDM) implemented in Satreps project can be used as a role model for Balai Sabo to apply that model for National-wide disaster management implementation. The Balai Sabo's crisis center activity for landslide and lahar early warning system is a tool to do so.

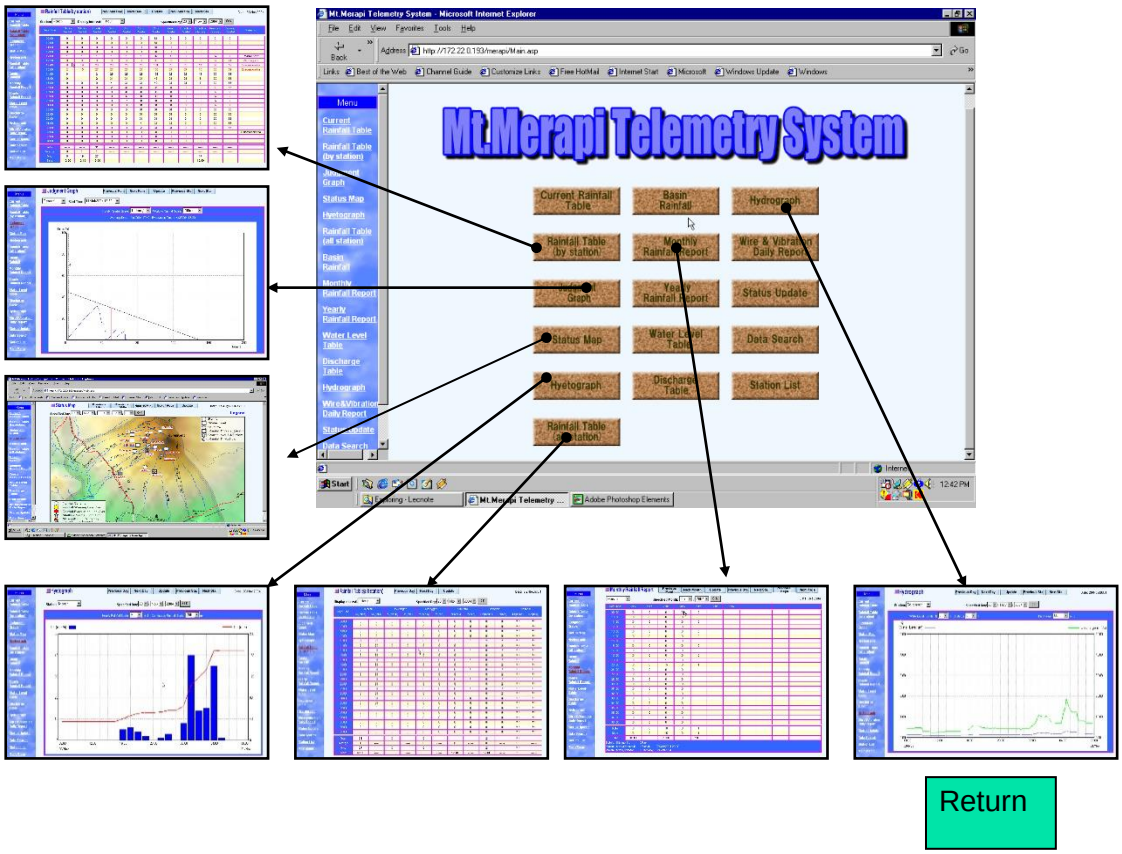

Return

One of activities work from Balai Sabo